A phosphorylation of RIPK3 kinase initiates an intracellular apoptotic pathway that promotes corpus luteum regression

Dianrong Li[1,2], Jie Chen[1,2], Jia Guo[1,2], Lin Li[1,2], Gaihong Cai[1,2], She Chen[1,2], Jia Huang[3], Hui Yang[3], Yinhua Zhuang[1,2], Fengchao Wang[1,2], and Xiaodong Wang[1,2,4,*]

[1]National Institute of Biological Sciences, Beijing 102206, China

[2]Tsinghua Institute of Multidisciplinary Biomedical Research, Tsinghua University, Beijing 100084, China

[3]Institute of Neuroscience, State Key Laboratory of Neuroscience, Key Laboratory of Primate Neurobiology, CAS Center for Excellence in Brain Science and Intelligence Technology, Shanghai Research Center for Brain Science and Brain-Inspired Intelligence, Shanghai Institutes for Biological Sciences, Chinese Academy of Sciences, Shanghai 200031, China

[4]Lead Contact

*Correspondence: wangxiaodong@nibs.ac.cn

Abstract

Receptor-interacting serine/threonine-protein kinase 3 (RIPK3) normally signals to necroptosis by phosphorylating MLKL. We report here that when the cellular RIPK3 chaperone Hsp90/CDC37 level is low, RIPK3 also signals to apoptosis. The apoptotic function of RIPK3 requires phosphorylation of the serine 165/threonine 166 sites on its kinase activation loop, resulting in inactivation of RIPK3 kinase activity while gaining the ability to recruit RIPK1, FADD, and caspase-8 to form a cytosolic caspase-activating complex, thereby triggering apoptosis. We found that $PGF_{2\alpha}$ induces RIPK3 expression in luteal granulosa cells in the ovary to cause luteal regression through this RIPK3-mediated apoptosis pathway. Mice carrying homozygous phosphorylation-resistant RIPK3 S165A/T166A knockin mutations failed to respond to $PGF_{2\alpha}$ but retained pro-necroptotic function, whereas mice with phospho-mimicking S165D/T166E homozygous knockin mutation underwent spontaneous apoptosis in multiple RIPK3-expressing tissues and died shortly after birth. Thus, RIPK3 signals to either necroptosis or apoptosis depending on its serine 165/threonine 166 phosphorylation status.

Introduction

Regulated cell death with distinctive associated morphological changes happens either in the form of apoptosis or necrosis (Elmore, 2007; Fink and Cookson, 2005; Kroemer et al., 2009; Wallach et al., 2016). Apoptosis is executed by intracellular caspases, particularly caspase-3, whose cleavage of several intracellular substrates gives rise to characteristic features of apoptotic cell death. Caspase-3 is activated by upstream caspase-8 or caspase-9, which are known to be activated respectively by being part of plasma membrane-associated death-inducing signaling complexes induced by the TNF

family of cytokines, or being part of the cytosolic apoptosome, which is formed as a result of cytochrome c release from mitochondria (Elmore, 2007; Li et al., 1997; Wang et al., 2008). Cells that die by apoptosis maintain their plasma membrane integrity and break down into small vesicles phagocytosed by macrophages (Elmore, 2007; Kroemer et al., 2009). Cells that die by regulated necrosis are executed by membrane-disrupting proteins that, when activated, translocate from the cytosol to the plasma membrane and disperse cellular contents into the cell surroundings. This process is often associated with inflammatory response (Christofferson and Yuan, 2010; Vandenabeele et al., 2010; Wallach et al., 2016).

One form of regulated necrosis, necroptosis, is executed by a pseudokinase namely mixed lineage kinase-domain protein, MLKL (Sun et al., 2012). MLKL is a substrate of receptor-interacting kinase RIPK3, which becomes activated either by: 1) the TNF family of cytokines through a related kinase RIPK1 that interacts with RIPK3 through a RIP homotypic interaction motif (RHIM) domain, or 2) by other RHIM domain-containing proteins, such as TRIF or ZBP1/DAI, that relay necroptotic signals from Toll-like receptors or intracellular Z-RNA, respectively (Cho et al., 2009; Degterev et al., 2008; He et al., 2009; Sun et al., 2012; Upton et al., 2012; Zhang et al., 2009; Zhang et al., 2020). Active RIPK3 phosphorylates MLKL at serine 357/threonine 358 (human origin) sites to induce oligomerization and translocation from the cytosol to the plasma membrane and cause loss of membrane integrity (Cai et al., 2014; Chen et al., 2014; Sun et al., 2012; Wang et al., 2014).

Surprisingly, a kinase-dead mutant RIPK3, D161N, spontaneously causes host cells to undergo apoptosis, resulting in embryonic lethality in mice bearing such homozygous mutation (Newton et al., 2014). On the other hand, mice homozygous with another kinase-dead mutant, K51A RIPK3, does not share this phenotype. However, cells that

harbor this mutation are sensitive to apoptosis induction when treated with several small-molecule RIPK3 inhibitors that bind to its ATP-binding pocket (Mandal et al., 2014). Whether this apoptosis-inducing activity of RIPK3 is an anomaly of the mutant protein, the small-molecule inhibitor bound form, or a true physiological function of RIPK3 remains to be resolved.

Apoptosis and necroptosis play important physiological and pathological roles in mammals (Christofferson and Yuan, 2010; Elmore, 2007; Vandenabeele et al., 2010; Wallach et al., 2016). Apoptosis has essential functions during animal development and maintaining cell homeostasis in adults (Elmore, 2007; Fink and Cookson, 2005). Necroptosis functions include anti-viral infections, tissue damage response, and male reproductive system aging (Cho et al., 2009; He and Wang, 2018; Li et al., 2017).

One of the important physiological functions of apoptosis in adult mammals is the development and function of the ovary (Perez et al., 1997; Rimon-Dahari et al., 2016; Rolaki et al., 2005; Tilly, 2001). From the neonatal stage to sex maturation, most eggs within primordial follicles fail to develop and undergo a process called atresia – a process driven by apoptosis of the egg and surrounding granulosa cells (Rimon-Dahari et al., 2016; Tilly and Sinclair, 2013). After sex maturation, follicles develop from primordial to primary and secondary follicles accompanied by the proliferation of surrounding granulosa and theca cells (Rimon-Dahari et al., 2016; Sanchez and Smitz, 2012; Tilly and Sinclair, 2013). After egg release from the follicle during ovulation, the remaining granulosa and theca cells become progesterone-producing sources, namely corpus luteum, which is easily recognizable under a microscope (Rolaki et al., 2005). If the egg is unfertilized, the corpus luteum dies through apoptosis and becomes corpus albicans, a scar tissue with a mixture of cell debris, macrophages, type I collagen, and fibroblasts and is light in color compared to the luteum. The process is also known as luteal involution or luteolysis (Rolaki et al., 2005;

Stocco et al., 2007; Tilly, 2001). Such a process stops the production of progesterone and triggers another cycle of ovulation. When mammals age, their follicles and corpora lutea are gradually lost, and the ovary eventually becomes a corpus albicans-filled organ that ceases to produce eggs and hormones (Perheentupa and Huhtaniemi, 2009; Tilly, 2001).

In the current study, we report that RIPK3 specifically induces apoptosis instead of necroptosis in certain contexts and cell types. The apoptosis-inducing function of RIPK3 requires the auto-phosphorylation of the evolutionarily conserved serine 165/threonine 166 sites (mouse origin) on its kinase activation loop, resulting in the inactivation of its kinase activity and acquiring the ability to recruit RIPK1-FADD-caspase-8, which leads to activation of caspase-3 and apoptosis. The apoptosis vs necroptosis function of RIPK3 seemed to be determined by the cellular level of a RIPK3 chaperone Hsp90/CDC37. We also found that the serine 165/threonine 166 phospho-RIPK3 signal specifically appeared in corpora lutea/albicans when mice reached more than 4-month of age and $PGF_{2\alpha}$ can specifically trigger this apoptotic pathway during the process of corpus luteum involution in a mouse hyper-ovulation model.

Results

Ectopic expression of RIPK3 in cultured MCF7 or human granulosa lutein cells activated apoptosis through the RIPK1-FADD-Caspase-8 pathway

We engineered three Dox-inducible RIPK3 expressing cell lines: HeLa/TO-RIPK3, MCF7/TO-RIPK3, and KGN/TO-RIPK3, all of which do not express endogenous RIPK3. KGN is a human granulosa tumor cell line (Nishi et al., 2001). Surprisingly we found that simple expression of RIPK3 in MCF7 or KGN cells caused cell death (Figure 1A and Figure 1-figure supplement 1), whereas the ectopic expression of RIPK3 in HeLa cells did not affect cell viability, similar to previous studies (Sun et al., 2012). Moreover, these

RIPK3-expressing MCF7 and KGN cells did not undergo necroptosis when we treated the cells with TSZ (TNF.α(T), a Smac mimetic (S), and a pan-caspase inhibitor Z-VAD-fml (Z)), whereas such treatment caused robust necroptosis in RIPK3-expressing HeLa cells (Figure 1B).

To determine what kind of cell death was triggered by RIPK3 in MCF7 and KGN cells, we used caspase inhibitor z-VAD-fmk, RIPK1 inhibitor RIPA-56 (Li et al., 2017), and MLKL inhibitor NSA (Sun et al., 2012) to co-treat these cells with Dox. Cell death induced by Dox could be blocked by caspase inhibitor z-VAD-fmk (Figure 1C and Figure 1-figure supplement 1) but not by MLKL inhibitor NSA, nor RIPK1 kinase inhibitor RIPA-56 (Figure 1C and Figure 1-figure supplement 1), indicating that the observed RIPK3-mediated cell death was apoptotic. However, this form of apoptosis did not signal through the classic intrinsic mitochondrial pathway, as the loss of cell viability through this pathway could not be blocked by caspase inhibitors, nor was the apoptosis triggered by the TNF receptor family, which would be RIPK1 kinase-dependent.

To further explore the molecular mechanism of this apoptosis pathway, we expressed a previously reported kinase-dead mutant (K50A) of RIPK3 in MCF7 cells and found that this kinase-dead mutant RIPK3(K50A) did not cause cell death (Figure 1D). Interestingly, the expression of this kinase-dead mutant RIPK3(K50A) plus RIPK3 kinase inhibitor GSK'872 resulted in robust apoptosis, similar to what was described by Mandal et al (Figure 1D; Mandal et al., 2014). Moreover, the mutations at the RHIM domain of RIPK3 known to disrupt RHIM-RHIM interaction also caused complete loss of cell death induction, indicating that RHIM domain interaction, possibly with another RHIM domain-containing protein, is required for apoptotic induction by RIPK3 (Figure 1D).

RIPK3's dependence on the RHIM domain but not its kinase activity suggested that the observed apoptosis might be through the RIPK1-FADD-caspase-8 pathway, as was

seen in apoptosis induced by the D161N mutant RIPK3, a kinase-dead mutant of RIPK3 that causes spontaneous apoptosis and prenatal lethality in mice carrying this knock-in mutation (Newton et al., 2014). We therefore immunoprecipitated the Flag-tagged RIPK3 and probed the immune-precipitate with antibodies against RIPK1, caspase-8, and FADD. Indeed, all three proteins were co-immunoprecipitated with RIPK3. The amount of RIPK1 and caspase-8 associated with RIPK3 increased when a caspase inhibitor was present, indicating the complex had increased stability when caspase-8 activity was blocked, presumably by preventing caspase-8-mediated cleavage of RIPK1, which serves as an adaptor protein between RIPK3 (through the RHIM domain) and FADD (through the DEAD domain) (Figure 2A; Mandal et al., 2014; Newton et al., 2014; Sun et al., 1999). When we used the CRISPR/Cas9 to knock out either *RIPK1*, *caspase-8*, or *FADD* gene in MCF7/TO-RIPK3 cells, we found that cell death upon addition of Dox was blocked entirely (Figure 2B-2D). Interestingly, different from the previous report (Mandal et al., 2014), knocking out the *cFLIP* gene did not block RIPK3 induced apoptosis in MCF7 cells but rather enhanced it (Figure 2E).

RIPK3 auto-phosphorylates serine164/threonine 165 in apoptotic cells

The differential apoptotic response of HeLa cells and MCF7/KGN cells to RIPK3 expression prompted us to search for the differences in RIPK3 protein in these cells. To this end, we immunoprecipitated Flag-RIPK3 from HeLa cells and MCF-7 cells and performed a detailed mass spectrometry analysis. We found two amino acid residues at the activation loop of the RIPK3 kinase domain, serine 164 and threonine 165, that were specifically phosphorylated in MCF7 cells but not in HeLa cells (Figure 3A). To validate this phosphorylation event, we generated a monoclonal antibody against the phopho-S164/T165 peptide. This phospho-specific antibody only recognized RIPK3

protein expressed in KGN or MCF7 cells but not in HeLa cells (Figure 3B). We further validated our monoclonal antibody's specificity by expressing a RIPK3 protein bearing phosphorylation-resistant mutations S164A/T165A in MCF and KGN cells. The expressed S164A/T165A RIPK3 was then analyzed by western blotting with antibodies against RIPK3 or phospho-S164/T165 RIPK3. As shown in Figure 3-figure supplement 1A and 1B, Dox-induced wild-type RIPK3 was recognized by anti-RIPK3 and anti-phospho-S164/T165 RIPK3 antibodies in both MCF7/TO-RIPK3 and KGN/TO-RIPK3 cells. The phosphorylation-resistant S164A/T165A mutant protein could only be recognized by the anti-RIPK3 antibody but not the anti-phospho-S614/T165 antibody. Notably, this anti-phospho-S164/T165 antibody did not recognize any non-specific protein band across the entire set of protein size markers (15-250 kDa), nor in cells without Dox addition to their media. Additionally, the expression of two kinase-dead mutants RIPK3 D160N and RIPK3 K50A (equivalent of mouse D161N and K51A, respectively) failed to generate the phospho-S164/T165 signal (Figure 3C and Figure 3-figure supplement 1C). Therefore, the RIPK3 induced apoptosis in KGN and MCF7 cells is dependent on the serine164/threonine 165 auto-phosphorylation of RIPK3 carried out by its own kinase activity.

Phosphorylation of serine164 inactivates the kinase activity of RIPK3 and activates apoptosis

To explore the functional significance of this phosphorylation event, we made phospho-mimic point mutations in these two sites and assayed the kinase activity of mutant RIPK3 by probing the serine 227 phosphorylation, which is known to be carried out by RIPK3 kinase activity and is critical for recruiting its necroptosis executing substrate MLKL (Li et al., 2015; Sun et al., 2012). After transiently transfecting the cDNA of mutant

RIPK3 in human embryonic kidney 293T cells, we observed that RIPK3 bearing phospho-mimic S164D/T165E mutations failed to auto-phosphorylate the serine 227 site, similar to the kinase-dead mutant D160N, whereas wild type RIPK3 readily phosphorylated serine 227 (Figure 3D).

We subsequently measured cell death after introducing these phospho-mimic or phosphorylation-resistant mutations in MCF7 and KGN cells. As shown in Figure 3E and 3F, introducing phospho-mimic mutations S164D/T165E increased apoptosis in MCF7 and KGN cells compared to wild-type RIPK3, whereas the phosphorylation-resistant mutant S164A/T165A lost the ability to induce apoptosis, similar to the RHIM domain mutant. Remarkably, in HeLa cells, the phospho-mimic mutant S164D/T165E gained the ability to induce apoptosis similar to the kinase-dead mutant D160N (Figure 3G), indicating that phospho-mimic mutations activated RIPK3's apoptosis-inducing function that is normally silenced in HeLa cells. Since the phospho-mimic mutations inactivate RIPK3 kinase activity, this S164D/T165E mutant was no longer able to induce necroptosis in HeLa cells when treated with necroptosis stimuli TSZ (Figure 3-figure supplement 1D). The phosphorylation resistant mutant S164A/T165A still allowed HeLa cells to respond to necroptosis induction, though the apoptosis-inducing function was lost in KGN and MCF7 cells (Figure 3-figure supplement 1D). Thus, the differential responses of RIPK3 in HeLa cells compared to KGN and MGF7 cells are due to its inability to carry out auto-phosphorylation at the serine 164/theorine165 sites.

We further narrowed down the effect of serine 164 and threonine 165 phosphorylation by generating individual phospho-mimic or phosphorylation-resistant mutants at serine S164 or threonine 165 sites and measured their kinase activity and apoptosis-inducing ability. The phospho-mimic S164E, but not T165E, mutant lost necroptosis responsiveness and gained the ability to induce apoptosis in HeLa cells, while phosphorylation resistant

S164A, but not T165A, lost its apoptosis-inducing activity in KGN and MCF7 cells (Figure 3-figure supplement 1D-1G). Together, these results indicated that RIPK3 auto-phosphorylation on the serine S164 site is a critical event that inactivates RIPK3 kinase activity while gaining apoptosis-inducing activity in KGN and MCF7 cells.

Serine 164 phosphorylation allows RIPK3 binding to RIPK1-FADD-Caspase-8

To study the mechanism by which phopho-S164/T165 RIPK3 activates the RIPK1/FADD/caspase-8 pathway, we ectopically expressed Flag-RIPK3 (wild type), phopho-mimic RIPK3 (S164D/T165E), and RIPK3 (D160N) kinase-dead mutants, as well as RIPK3(AAAA) RHIM domain mutants in HeLa cells and performed immunoprecipitation with an anti-Flag antibody. The immune-complexes were probed with antibodies against RIPK1, FADD, and caspase-8. As shown in Figure 3H, very little RIPK1, FADD, or caspase-8 were co-precipitated with wild type or RHIM mutant RIPK3, consistent with its inability to induce apoptosis (Figure 3H, lanes 1 and 2). In contrast, two kinase-dead mutants, either the artificial D160N or phospho-mimic S164D/T165E, showed robust binding with RIPK1, FADD, and caspase-8 (Figure 3H, lanes 3 and 4). Consistent with the cell death result, the phosphorylation-resistant mutant S164A/T165A lost the ability to bind with RIPK1, FADD, and caspase-8 (Figure 3I).

Consistent with the finding that the serine 164 phosphorylation is most critical for RIPK3 apoptosis-inducing activity, the phospho-mimic S164E mutant expressed in HeLa cells was found to associate with RIPK1, FADD, and caspase-8, as did the S164D/T165E double mutation (Figure 3-figure supplement 1H, lane 4), whereas T165E alone could not bind to these proteins (Figure 3-figure supplement 1H, lane 2). Collectively, these findings indicate that RIPK3 auto-phosphorylation on serine S164 allows RIPK3 to recruit RIPK1

to form the RIPK3/RIPK1/FADD/Caspase-8 complex, in which caspase-8 is activated to drive apoptosis.

Hsp90/CDC37 chaperone determines the necroptotic or apoptotic function of RIPK3 kinase

We have previously observed that in order for RIPK3 to signal to necroptosis, the protein needs to be correctly folded with the aid of a molecular chaperone consisting of Hsp90 and CDC37 (Li et al., 2015). In HT29 and HeLa cells in which RIPK3 signals primarily to necroptosis, we observed that the level of Hsp90/CDC37 was higher compared to MCF7 and KGN cells, where RIPK3 predominantly causes apoptosis (Figure 4A). Indeed, a human Hsp90 inhibitor 17AAG potently blocked necroptosis induced by TSZ in HeLa-RIPK3 cells, whereas 17AAG did not block RIPK3 induced apoptosis in MCF7/TO-RIPK3 or KGN/TO-RIPK3 cells (Figure 4B and 4C). When we knocked down Hsp90 using shRNA or inhibits Hsp90 using 17AAG, after Dox induce RIPK3 expression, we saw the switch of the cellular necroptosis response to apoptosis (Figure 4D and Figure 4-figure supplement 1A). Consistently, the serine 164/threonine 165 phosphorylation of RIPK3 also occurred after the inhibition of Hsp90 (Figure 4E). Reciprocally, when Hsp90 and CDC37 were ectopically expressed in MCF7/TO-RIPK3 cells to a level matched or exceeding that in HeLa cells, the serine 164/threonine 165 phosphorylation of RIPK3 no longer occurred, and RIPK3-mediated apoptosis induction mostly ceased (Figure 4F and 4G). Consistent with the cell death result, when the inhibitor of Hsp90 17AAG was present during RIPK3 induction in HeLa/TO-RIPK3 cells, the RIPK3 formed a complex with RIPK1, FADD, and caspase-8 (Figure 4H).

Since serine 164/threonine 165 appeared to be at a critical regulatory region in RIPK3 on which phosphorylation switches its function from necroptosis to apoptosis, we checked

this region among different mammalian species. As shown in Figure 3-figure supplement 2A, this region is conserved with no changes from amino acid residues 160-174 among RIPK3s from human, chimpanzee, rat, mouse, and bovine origin (Xie et al., 2013). The corresponding phospho-mimic mutations of mouse RIPK3(S165D/T166E), like RIPK3(D161N) kinase-dead mutants (Newton et al., 2014), failed to auto-phosphorylate the serine 232 site, the equivalent of the human serine 227 site (Figure 3-figure supplement 2B). Furthermore, these mutant RIPK3 proteins induced apoptosis in mouse L929 (*Ripk3*$^{-/-}$) cells after ectopic expression but not necroptosis when treated with the necroptosis stimulus TSZ (Figure 3-figure supplement 2C). Previously, we noticed that when we used a clinical relevant dose of 17AAG (200 nM) to treat mouse cells, the necroptosis was augmented instead of inhibited like in human or rat cells (Li et al., 2015). We therefore suggested that the Hsp90/CDC37 chaperone might not work in mouse cells. Given the importance of this chaperone system in determining the apoptotic or necroptotic fate and the conservation of the apoptosis-causing phosphorylation site in mice, we explored the possibility that the previously tested concentration of human Hsp90 inhibitors was simply not enough to inhibit the mouse Hsp90. Indeed, when the higher dose of 17AAG was used, the compound dose-dependently blocked TSZ-induced necroptosis in L929 cells (Figure 4-figure supplement 1B). Moreover, when we knocked down Hsp90 using shRNA or inhibits Hsp90 using higher concentrations of 17AAG in L929 (*Ripk3*$^{-/-}$)/TO-RIPK3 cells, we saw the switch of the cellular necroptosis response to apoptosis after Dox induced RIPK3 expression (Figure 4-figure supplement 1C and 1D). The serine 165/threonine 166 phosphorylation of RIPK3 also occurred after the inhibition of Hsp90 (Figure 4-figure supplement 1E). These results indicated that the observed Hsp90/CDC37-determined, RIPK3 serine 164/threonine 165 phosphorylation-driven apoptosis is conserved between human and mouse cells.

RIPK3 forms a unique structure in MCF7 and KGN cells

RIPK3 is known to form diffused puncta within the cytosol (He et al., 2009). Indeed, when the HeLa/TO-RIPK3 cells were treated with Dox plus TSZ, we observed expressed RIPK3 in diffused puncta in the cytosol (Figure 4-figure supplement 2A). Interestingly, when we performed a similar analysis of RIPK3 distribution in MCF7/TO-RIPK3 and KGN/TO-RIPK3 cells, the RIPK3 formed a high order of structures distinct from the diffused punctae in HeLa or HT29 cells (Figure 4-figure supplement 2A and 2B). Furthermore, the phospho-S164/T165-RIPK3 signal appeared co-localized with RIPK3 in MCF7 cells but no such signal was seen in HeLa cells (Figure 4-figure supplement 2C). The formation of these high order structures and the appearance of the phospho-S164/T165-RIPK3 signal was not affected when *RIPK1*, *caspase-8*, or *FADD* genes were knocked out (Figure 4-figure supplement 2D and 2E).

To test whether this high order structure of RIPK3 is associated with its ability to induce apoptosis, we treated the HeLa/TO-RIPK3 cells with Dox plus the Hsp90 inhibitor 17AAG and found that the diffused punctae of RIPK3 were now switched to the high order structure (Figure 4I). Reciprocally, when Hsp90 and CDC37 were ectopically overexpressed in MCF7/TO-RIPK3 cells, the high order structure of RIPK3 became diffused punctae throughout the cytosol of the cells (Figure 4J). These findings collectively indicated that RIPK3 forms distinctive cellular structures when signaling to apoptosis or necroptosis, depending on the chaperone Hsp90/CDC37.

Ripk3$^{S165D\text{-}T166E/S165D\text{-}T166E}$ mice die within a month after birth due to spontaneous apoptosis in multiple tissues

We subsequently sought genetic proof that the phosphorylation of RIPK3 at its serine 165/threonine 166 sites (equivalent to human serine164/threonine165 sites) drives apoptosis *in vivo*. To this end, we generated *Ripk3* knock-in mice with $Ser^{165}Thr^{166}$ mutated to Ala-Ala or Asp-Glu (Figure 5-figure supplement 1A, 1B, and 1E) to either block or mimic the phosphorylation on these sites (Figure 5-figure supplement 1A, 1B, and 1F). Interestingly, the $Ripk3^{S165A-T166A/S165A-T166A}$ homozygous mice were viable and appeared normal (Figure 5-figure supplement 1C, 1D, and 1F). $Ripk3^{S165D-T166E/S165D-T166E}$ homozygous mice, on the other hand, are smaller in size and all died within one month after birth (Figure 5A-5C). Anatomical analysis of these $Ripk3^{S165D-T166E/S165D-T166E}$ mice showed abnormal large intestine, small intestine, lung, spleen, and kidney, while other major organs, including brain, cerebellum, heart, and liver, appeared normal (Figure 5D and Figure 5-figure supplement 1G). Staining for cleaved caspase-3 revealed significantly increased apoptosis in the large intestine, small intestine, lung, and spleen (Figure 5E and 5F). The $Ripk3^{S165D-T166E/+}$ heterozygous mice, which were expected to make half the amount of RIPK3 S165D/T166E protein, are viable, indicating that there must be a threshold above which the RIPK3 S165D/T166E protein becomes lethal.

Consistent with what was seen in HeLa cells, in which the phospho-mimic mutations S164D/T165E of RIPK3 were unable to signal necroptosis, the bone marrow-derived macrophages (BMDM) from $Ripk3^{S165D-T166E/S165D-T166E}$ mice were resistant to necroptosis induction by TSZ (Figure 5G). Conversely, the BMDM from $Ripk3^{S165A-T166A/S165A-T166A}$ mice readily underwent necroptosis when treated with TSZ, as did the BMDM from wild type mice (Figure 5-figure supplement 1H).

$PGF_{2\alpha}$ elevates the expression of RIPK3 in luteal granulosa cells to promote luteum regression

Among all RIPK3 expressing tissues, RIPK3 expression levels in the ovary were the most notable, following a reversed bell curve pattern through the lifetime of the mice (Figure 6A). In early life and young adulthood, RIPK3 expression was restricted to the follicle granular cells around the egg (Figure 6B). In later life, RIPK3 protein starts to appear in the corpus luteum and albican (Figure 6B). The second wave of expression coincides with the elevation of prostaglandin F2alpha ($PGF_{2\alpha}$), which has been reported to have a role in apoptosis induction during luteal involution (Parkening et al., 1985). Indeed, when we measured the $PGF_{2\alpha}$ levels in the mouse ovary, we saw a significant age-dependent increase as mice aged from 4 months to 10 and 16 months, coinciding with the age-dependent elevation of RIPK3 (Figure 6C). Moreover, when we co-stained 12-month-old RIPK3-Flag knock-in ovaries with anti-Flag and prostaglandin F receptor (PTGFR), we noticed that the PTGFR signal was primarily located in corpus lutea and corpus albicans but not in the follicles and co-localized with that of RIPK3 (Figure 6D and Figure 6-figure supplement 1).

We thus used the same anti-phospho-S164/T165 antibody to probe ovary extracts from mice of different ages by western blotting. We found no phosphorylation signal in young (2-month old) ovaries, despite the RIPK3 protein band being readily detectable (Figure 6E). The signal began to appear at 4 months and gradually increased when mice advanced in age (Figure 6E). To locate this phosphorylation signal in aged ovaries, we used this antibody for immunohistochemical analysis on 4, 8, and 12-month-old ovaries. Consistent with the western blotting, there was minimal signal in the young (4-month old) ovary. There were patches of signal in 8-month-old corpus luteum and albican, and the signal became prominent and clustered in the corpus albicans in 12-month-old ovary (Figure 6F, middle panels). In contrast, no such phospho-RIPK3 signal was seen in 12-month-old ovaries of RIPK3 knockout mice, further confirming the specificity of this monoclonal antibody (Figure 6F).

RIPK3 induce apoptosis or necroptosis depending on the chaperone Hsp90/CDC37 level *in vitro*. To measure the level of Hsp90/CDC37 in granulosa cells of follicles and corpus lutea/albicans, we did immunofluorescence staining of 8-month old mouse ovaries

using antibodies against these two proteins. Both antibodies stained follicle granulosa much more strongly than corpus lutea and albicans, whereas RIPK3 staining signal was at a similar level in both, indicating that the relative level of Hsp90/CDC37 vs RIPK3 is higher in follicles than corpus lutea and albicans (Figure 4-figure supplement 3). Collectively, these results suggested that RIPK3-induced apoptosis in aged corpus lutea and albicans was due to lower levels of Hsp90/CDC37 chaperone in these regions of the ovary.

$PGF_{2\alpha}$ is known to stimulate the Raf/MEK1/Mitogen-activated protein kinase signaling pathway to induce luteal regression (Chen et al., 1998; Rolaki et al., 2005; Wang et al., 2003; Yadav et al., 2002). In mice, knockout caspase-3 blocks $PGF_{2\alpha}$–induced regression of the corpus luteum (Carambula et al., 2002; Carambula et al., 2003). Those observations suggested that $PGF_{2\alpha}$ might induce RIPK3 expression by stimulating the Raf/MEK1/Mitogen-activated protein kinase signaling pathway, thus causes RIPK3-mediated apoptosis. To test if $PGF_{2\alpha}$ could directly induce RIPK3 expression, we isolated primary granulosa lutein cells from young (3 months old) mouse ovaries and treated them with a synthetic $PGF_{2\alpha}$ analog dinoprost tromethamine (DT) (Chebel et al., 2007). We then observed the time and dose-dependent induction of RIPK3 protein, a pattern that overlapped with the appearance of phospho-ERK/MEK signal, an indication of PGF2 receptor activation (Figure 7A and 7B). The addition of two MEK kinase inhibitors PD-98059 or U0126 blocked RIPK3 induction, confirming that the RIPK3 induction by $PGF_{2\alpha}$ was indeed through the MEK pathway (Figure 7-figure supplement 1A). Importantly, the DT-induced RIPK3 was phosphorylated at its serine 165/threonine166 sites, and the treated cells were undergoing apoptosis, as indicated by the presence of active caspase-3 (Figure 7C and Figure 7-figure supplement 1B). Consistent with the notion that apoptosis induced by $PGF_{2\alpha}$ is RIPK3 dependent, the primary granulosa lutein cells isolated from the RIPK3 knockout mice failed to respond to PGF2α activate caspase-3 (Figure 7C).

The ability of primary granulosa lutein cells from young animals to undergo RIPK3-mediated apoptosis in response to $PGF_{2\alpha}$ allowed us to genetically verify the role of the RIPK3-RIPK1-FADD-Caspase-8 pathway in luteum regression. To this end, we first induced hyper-ovulation in young female mice 4 weeks of age with gonadotropins and then treated them with DT as previously described (Carambula et al., 2002; Carambula et al., 2003; Figure 7-figure supplement 1C). The hyper-ovulation induced by gonadotropins generated multiple corpus lutea in the ovaries of these young mice (Figure 7D). The subsequent DT treatment induced the elevation of RIPK3 protein in their corpus lutea, and the induced RIPK3 was phosphorylated at the serine 164/threonine165 sites (Figure 7D and 7E). Moreover, the treatment of DT caused active caspase-3 signal to appear in the corpus lutea of wild-type ovaries (Figure 7F and 7G). Mice with their *PTGFR* gene knocked out failed to elevate the RIPK3 level in response to $PGF_{2\alpha}$ (Figure 7E and Figure 6-figure supplement 1). Although DT treatment induced the elevation of phosphorylation resistant RIPK3(S165A/T166A) protein in the ovaries of $Ripk3^{S165A\text{-}T166A/S165A\text{-}T166A}$ knockin mice to the same level as wild type RIPK3 protein (Figure 7-figure supplement 1D), significantly less active caspase-3 signal was observed in these ovaries, similar to the ovaries of $Ripk3^{-/-}$, $Fadd^{-/-}/Mlkl^{-/-}$, or $Ptgfr^{-/-}$ mice, confirming that the observed DT-induced apoptosis in luteal cells was through the RIPK3/FADD-mediated apoptosis pathway triggered by the phosphorylation of serine 165/threonine 166 sites (Figure 7F and 7G). We further co-stained the ovaries with antibodies against active caspase-3 and phopho-S165/T166 RIPK3 and found that most of the positive signals were overlapping (Figure 7H), indicating that serine165/threonine166 phosphorylated RIPK3 activates apoptosis in corpus luteum, triggered by $PGF_{2\alpha}$. Interestingly, although significantly lower overall, there was more active caspase-3 in $Ripk3^{-/-}$ and $Ripk3^{S165A\text{-}T166A/S165A\text{-}T166A}$ ovaries than in $Fadd^{-/-}/Mlkl^{-/-}$ ovaries, suggesting that there might be a redundant

RIPK3-independent but FADD-dependent apoptosis pathway that also functions in resolving the corpus luteum in this model. This residue cell death could be through the classic extrinsic apoptosis pathway described previously (Carambula et al., 2003; Hu et al., 2001). Collectively, these results demonstrated that most of the corpus luteum involution induced by $PGF_{2\alpha}$ is indeed through the RIPK3-RIPK1/FADD/Caspase-8 pathway triggered by RIPK3 induction and phosphorylation at serine 165/threonine 166.

Discussion

The function of RIPK3 in apoptosis and necroptosis is controlled by auto-phosphorylation of the amino acid residue serine 164

The apoptotic role of RIPK3 has been observed ever since RIPK3 was first identified (Sun et al., 1999). The initial characterization of RIPK3, mainly by ectopic overexpression, indicated that it functioned in apoptosis (Sun et al., 1999). Later, however, RIPK3 was identified as a key signaling molecule for necroptosis due to its ability to specifically phosphorylate MLKL, the executioner of this form of cell death (Cho et al., 2009; He et al., 2009; Zhang et al., 2009; Sun et al., 2012). The debate of the apoptotic or necroptotic role of RIPK3 was further brought to the front by the observation that the D161N mutation of RIPK3 (D160N of human origin), a mutation that takes out the key DFG motif of the kinase active site and renders RIPK3 kinase-inactive, caused spontaneous apoptosis by activating caspase-8 through RIPK1 and FADD (Newton et al., 2014). Yet surprisingly, another kinase-dead mutant of RIPK3, the K51A mutant, does not induce apoptosis like D161N, but instead only starts to signal to apoptosis in the presence of small-molecule RIPK3 kinase inhibitors that occupy the ATP-binding site of the kinase domain (Mandal et al., 2014). These observations suggest that it is not the inactivation of kinase activity *per se* that switches RIPK3 function from necroptosis to apoptosis. It is more likely the

conformational change that happens due to particular mutations or kinase inhibitor binding that triggered such a change. We now understand that this change of RIPK3 function from pro-necroptotic to apoptotic most likely mimicked the specific phosphorylation at the serine 164 (mouse 165) site, carried out by RIPK3 kinase itself. The serine 164 amide nitrogen forms a conserved H-bond with the carbonyl oxygen of phenylalanine 160 (part of the DFG motif of kinase), a feature important to maintain the RIPK3 active configuration (Xie et al., 2013). Introducing a phosphate group at this site conceivably disrupts this critical interaction, resulting in loss-of-function of the RIPK3 kinase and a conformational change that allows the RHIM domain to be available for RHIM-RHIM interaction between RIPK3 and RIPK1. Since it is the amide, not the side chain of serine 164 that participates in maintaining the active configuration of RIPK3, it is not surprising that the phosphorylation-resistant mutant S164A/T165A retains the kinase activity and is still able to signal to necroptosis, although such a mutation loses its apoptosis-inducing activity. Interestingly, RIPK1 kinase functions here purely as an adaptor for the recruitment of FADD and caspase-8, and its kinase activity is not required for this apoptosis function. Therefore, unlike the apoptosis and necroptosis-inducing functions of RIPK1 when it responds to the TNF receptor family of proteins, the apoptosis-inducing activity of RIPK1 that is initiated by RIPK3 phosphorylation is not sensitive to RIPK1 kinase inhibitors.

Although we cannot completely rule out the possibility of another yet to be identified kinase(s) that carries out the phosphorylation of serine 164/threonine 165 of RIPK3, our current data favor the idea that the phosphorylation is catalyzed by RIPK3 itself. Both D160N and K50A kinase dead mutant RIPK3 failed to generate the phospho-Serine164/Threonine 165 signal (Figure 3C and Figure 3-figure supplement 3C). Especially, the K50 site is not in the proximity of the S164/T165 phosphorylation sites, thus, the loss of phosphorylation is unlikely due to interference with substrate recognition

that might have occurred with the D160N mutant, if the phosphorylation is carried out by another kinase.

The level of RIPK3 chaperone Hsp90/CDC37 determines the cellular necroptotic or apoptotic function of RIPK3

Our investigation has now clearly shown that RIPK3 naturally has dual roles in both necroptosis and apoptosis. In cells in which the RIPK3 kinase predominantly signals to necroptosis, like in human colon cancer HT29 cells, the RIPK3 chaperone Hsp90/CDC37 level is relatively high, which allows RIPK3 to fold into a configuration that can only be activated by upstream signaling molecules, be that either RIPK1 in response to TNF receptor family members, or TRIF and ZBP1/DAI in response to toll-like receptors or Z-RNA, respectively. In this case, RIPK3 kinase activity is silent, and no auto-phosphorylation signal or downstream substrate MLKL phosphorylation occurs before upstream activation signals arrive.

However, in cells in which Hsp90/CDC37 chaperone level is relatively low or artificially inhibited by Hsp90 inhibitors, the newly generated RIPK3, either by artificial induction (through transient transfection or Dox-induced expression) or by physiological signals like $PGF_{2\alpha}$, can auto-phosphorylate its serine 164/threonine 165 sites of its conserved kinase activation loop, triggering apoptosis by forming the RIPK3-RIPK1-FADD-Caspase-8 complex, leading to caspase-8 activation. Indeed, mice bearing the phospho-mimic mutations of these sites (S165D/T166E) showed spontaneous activation of apoptosis in all RIPK3-expressing tissues, including lung, intestines, and spleen, and these mice die within a month after birth.

We noticed previously that Hsp90 inhibitors developed against human Hsp90 did not block necroptosis in mouse bone marrow-derived macrophages but was efficacious in

BMDM from rat (Li et al., 2015). We now know that such a difference is mainly due to species specificity of these Hsp90 inhibitors. Using higher concentrations of human Hsp90 inhibitor 17AAG or knockdown Hsp90 protein in mouse cells, we recapitulated the similar necroptosis to apoptosis switch as in human cells (Figure 4-figure supplement 4B-4E). We thus realized that the previous conclusion that Hsp90/CDC37 chaperone system is not working in mouse cells is wrongly drawn due to lower efficacy of the Hsp90 inhibitors tested, which was developed to inhibit human Hsp90 (Li et al., 2015). The chaperone level of Hsp90/CDC37 is important to dictate the necroptotic or apoptotic function of mouse RIPK3 as well. Consistently, the levels of Hsp90 and CDC37 in the mouse luteum granulosa is much lower than that in the follicle granulosa (Figure 4-figure supplement 3).

Serine 164/threonine 165 phosphorylation of RIPK3 seems to be a unique biomarker for this RIPK3-mediated apoptosis pathway. Our development of a monoclonal antibody that specifically recognizes this phosphorylation event should be useful to identify tissues and cells in which this pathway is activated.

$PGF_{2\alpha}$ induces RIPK3-mediated apoptosis in luteal granulosa cells for luteum regression

One of the tissues in which this specific anti-phospho-S164/T165 monoclonal antibody picked up a signal was in luteal granulosa cells of aged mouse ovary. The appearance of this phopho-RIPK3 signal in the ovary coincident with the elevation of $PGF_{2\alpha}$ level and indeed, an analog of $PGF_{2\alpha}$ was able to induce the expression of S165/T166 phosphorylated RIPK3 in the primary granulosa cells from ovaries of young mice (Figure 7). The phenomenon of $PGF_{2\alpha}$–induced RIPK3-expression in the mouse ovary granulosa cells allowed us to genetically validate this intracellular apoptotic pathway. In a hyper-ovulation model in which many egg follicles from young mice were

induced to mature simultaneously, the accumulated granulosa cells in the ovary of wild type mice can be triggered into resolution by an agonist (DT) of $PGF_{2\alpha}$ through RIPK3-mediated apoptosis. However, DT could not induce apoptosis and luteum resolution in the ovary of PGF receptor knockout, RIPK3 knockout, FADD/MLKL double knockout, and *Ripk3*$^{S165A-T166A/S165A-T166A}$ knockin mice, confirming this intracellular pathway of apoptosis *in vivo*.

Although the RIPK3-mediated apoptosis can be recapitulated in this hyper-ovulation model using young mice, the serine 165/threonine 166 phospho-RIPK3 signal only naturally appears in luteal granulosa cells when mice reach a certain age. The RIPK3 knockout and *Ripk3*$^{S165A-T166A/S165A-T166A}$ knockin mice do not show any fertility defect in their normal reproductive age, indicating that the RIPK3-mediated apoptotic pathway does not have a critical role in luteum resolution when the mice are young. It is thus interesting to speculate that such a pathway may have a specific role during mouse ovary aging when all corpora lutea eventually become albicans.

References

Cai, Z., Jitkaew, S., Zhao, J., Chiang, H.C., Choksi, S., Liu, J., Ward, Y., Wu, L.G., and Liu, Z.G. (2014). Plasma membrane translocation of trimerized MLKL protein is required for TNF-induced necroptosis. Nat Cell Biol *16*, 55-65.

Carambula, S.F., Matikainen, T., Lynch, M.P., Flavell, R.A., Goncalves, P.B., Tilly, J.L., and Rueda, B.R. (2002). Caspase-3 is a pivotal mediator of apoptosis during regression of the ovarian corpus luteum. Endocrinology *143*, 1495-1501.

Carambula, S.F., Pru, J.K., Lynch, M.P., Matikainen, T., Goncalves, P.B., Flavell, R.A., Tilly, J.L., and Rueda, B.R. (2003). Prostaglandin F2alpha- and FAS-activating

554 antibody-induced regression of the corpus luteum involves caspase-8 and is defective in
555 caspase-3 deficient mice. Reprod Biol Endocrinol *1*, 15.
556 Chebel, R.C., Santos, J.E., Rutigliano, H.M., and Cerri, R.L. (2007). Efficacy of an
557 injection of dinoprost tromethamine when given subcutaneously on luteal regression in
558 lactating Holstein cows. Theriogenology *67*, 590-597.
559 Chen, D.B., Westfall, S.D., Fong, H.W., Roberson, M.S., and Davis, J.S. (1998).
560 Prostaglandin F2alpha stimulates the Raf/MEK1/mitogen-activated protein kinase
561 signaling cascade in bovine luteal cells. Endocrinology *139*, 3876-3885.
562 Chen, X., Li, W., Ren, J., Huang, D., He, W.T., Song, Y., Yang, C., Li, W., Zheng, X.,
563 Chen, P., *et al.* (2014). Translocation of mixed lineage kinase domain-like protein to
564 plasma membrane leads to necrotic cell death. Cell Res *24*, 105-121.
565 Cho, Y.S., Challa, S., Moquin, D., Genga, R., Ray, T.D., Guildford, M., and Chan, F.K.
566 (2009). Phosphorylation-driven assembly of the RIP1-RIP3 complex regulates
567 programmed necrosis and virus-induced inflammation. Cell *137*, 1112-1123.
568 Christofferson, D.E., and Yuan, J. (2010). Necroptosis as an alternative form of
569 programmed cell death. Curr Opin Cell Biol *22*, 263-268.
570 Degterev, A., Hitomi, J., Germscheid, M., , I.L., Korkina, O., Teng, X., Abbott, D., Cuny,
571 G.D., Yuan, C., Wagner, G., *et al.* (2008). Identification of RIP1 kinase as a specific
572 cellular target of necrostatins. Nat Chem Biol *4*, 313-321.
573 Elmore, S. (2007). Apoptosis: a review of programmed cell death. Toxicol Pathol *35*,
574 495-516.
575 Fink, S.L., and Cookson, B.T. (2005). Apoptosis, pyroptosis, and necrosis: mechanistic
576 description of dead and dying eukaryotic cells. Infect Immun *73*, 1907-1916.

He, S., Wang, L., Miao, L., Wang, T., Du, F., Zhao, L., and Wang, X. (2009). Receptor interacting protein kinase-3 determines cellular necrotic response to TNF-alpha. Cell *137*, 1100-1111.

He, S., and Wang, X. (2018). RIP kinases as modulators of inflammation and immunity. Nat Immunol *19*, 912-922.

Hu, C.L., Cowan, R.G., Harman, R.M., Porter, D.A., and Quirk, S.M. (2001). Apoptosis of bovine granulosa cells after serum withdrawal is mediated by Fas antigen (CD95) and Fas ligand. Biol Reprod *64*, 518-526.

Kroemer, G., Galluzzi, L., Vandenabeele, P., Abrams, J., Alnemri, E.S., Baehrecke, E.H., Blagosklonny, M.V., El-Deiry, W.S., Golstein, P., Green, D.R., *et al.* (2009). Classification of cell death: recommendations of the Nomenclature Committee on Cell Death 2009. Cell Death Differ *16*, 3-11.

Li, D., Meng, L., Xu, T., Su, Y., Liu, X., Zhang, Z., and Wang, X. (2017). RIPK1-RIPK3-MLKL-dependent necrosis promotes the aging of mouse male reproductive system. Elife *6*.

Li, D., Xu, T., Cao, Y., Wang, H., Li, L., Chen, S., Wang, X., and Shen, Z. (2015). A cytosolic heat shock protein 90 and cochaperone CDC37 complex is required for RIP3 activation during necroptosis. Proc Natl Acad Sci U S A *112*, 5017-5022.

Li, P., Nijhawan, D., Budihardjo, I., Srinivasula, S.M., Ahmad, M., Alnemri, E.S., and Wang, X. (1997). Cytochrome c and dATP-dependent formation of Apaf-1/caspase-9 complex initiates an apoptotic protease cascade. Cell *91*, 479-489.

Mandal, P., Berger, S.B., Pillay, S., Moriwaki, K., Huang, C., Guo, H., Lich, J.D., Finger, J., Kasparcova, V., Votta, B., *et al.* (2014). RIP3 induces apoptosis independent of pronecrotic kinase activity. Mol Cell *56*, 481-495.

Newton, H., Picton, H., and Gosden, R.G. (1999). In vitro growth of oocyte-granulosa cell complexes isolated from cryopreserved ovine tissue. J Reprod Fertil *115*, 141-150.

Newton, K., Dugger, D.L., Wickliffe, K.E., Kapoor, N., de Almagro, M.C., Vucic, D., Komuves, L., Ferrando, R.E., French, D.M., Webster, J., *et al.* (2014). Activity of protein kinase RIPK3 determines whether cells die by necroptosis or apoptosis. Science *343*, 1357-1360.

Nishi, Y., Yanase, T., Mu, Y., Oba, K., Ichino, I., Saito, M., Nomura, M., Mukasa, C., Okabe, T., Goto, K., *et al.* (2001). Establishment and characterization of a steroidogenic human granulosa-like tumor cell line, KGN, that expresses functional follicle-stimulating hormone receptor. Endocrinology *142*, 437-445.

Parkening, T.A., LaGrone, L.F., and Brouhard, B.H. (1985). Concentrations of prostaglandins in plasma, seminal vesicles, and ovaries of aging C57BL/6NNia mice. Exp Gerontol *20*, 291-294.

Perez, G.I., Knudson, C.M., Leykin, L., Korsmeyer, S.J., and Tilly, J.L. (1997). Apoptosis-associated signaling pathways are required for chemotherapy-mediated female germ cell destruction. Nat Med *3*, 1228-1232.

Perheentupa, A., and Huhtaniemi, I. (2009). Aging of the human ovary and testis. Mol Cell Endocrinol *299*, 2-13.

Rimon-Dahari, N., Yerushalmi-Heinemann, L., Alyagor, L., and Dekel, N. (2016). Ovarian Folliculogenesis. Results Probl Cell Differ *58*, 167-190.

Rolaki, A., Drakakis, P., Millingos, S., Loutradis, D., and Makrigiannakis, A. (2005). Novel trends in follicular development, atresia and corpus luteum regression: a role for apoptosis. Reprod Biomed Online *11*, 93-103.

Sanchez, F., and Smitz, J. (2012). Molecular control of oogenesis. Biochim Biophys Acta *1822*, 1896-1912.

626 Stocco, C., Telleria, C., and Gibori, G. (2007). The molecular control of corpus luteum
627 formation, function, and regression. Endocr Rev *28*, 117-149.
628 Sun, L., Wang, H., Wang, Z., He, S., Chen, S., Liao, D., Wang, L., Yan, J., Liu, W., Lei, X.,
629 *et al.* (2012). Mixed lineage kinase domain-like protein mediates necrosis signaling
630 downstream of RIP3 kinase. Cell *148*, 213-227.
631 Sun, X., Lee, J., Navas, T., Baldwin, D.T., Stewart, T.A., and Dixit, V.M. (1999). RIP3, a
632 novel apoptosis-inducing kinase. J Biol Chem *274*, 16871-16875.
633 Tian, Y., Shen, W., Lai, Z., Shi, L., Yang, S., Ding, T., Wang, S., and Luo, A. (2015).
634 Isolation and identification of ovarian theca-interstitial cells and granulose cells of
635 immature female mice. Cell Biol Int *39*, 584-590.
636 Tilly, J.L. (2001). Commuting the death sentence: how oocytes strive to survive. Nat Rev
637 Mol Cell Biol *2*, 838-848.
638 Tilly, J.L., and Sinclair, D.A. (2013). Germline energetics, aging, and female infertility.
639 Cell Metab *17*, 838-850.
640 Upton, J.W., Kaiser, W.J., and Mocarski, E.S. (2012). DAI/ZBP1/DLM-1 complexes with
641 RIP3 to mediate virus-induced programmed necrosis that is targeted by murine
642 cytomegalovirus vIRA. Cell Host Microbe *11*, 290-297.
643 Vandenabeele, P., Galluzzi, L., Vanden Berghe, T., and Kroemer, G. (2010). Molecular
644 mechanisms of necroptosis: an ordered cellular explosion. Nat Rev Mol Cell Biol *11*,
645 700-714.
646 Wallach, D., Kang, T.B., Dillon, C.P., and Green, D.R. (2016). Programmed necrosis in
647 inflammation: Toward identification of the effector molecules. Science *352*, aaf2154.
648 Wang, H., Sun, L., Su, L., Rizo, J., Liu, L., Wang, L.F., Wang, F.S., and Wang, X. (2014).
649 Mixed lineage kinase domain-like protein MLKL causes necrotic membrane disruption
650 upon phosphorylation by RIP3. Mol Cell *54*, 133-146.

651 Wang, L., Du, F., and Wang, X. (2008). TNF-alpha induces two distinct caspase-8
652 activation pathways. Cell *133*, 693-703.
653 Wang, Z., Tamura, K., Yoshie, M., Tamura, H., Imakawa, K., and Kogo, H. (2003).
654 Prostaglandin F2alpha-induced functional regression of the corpus luteum and apoptosis in
655 rodents. J Pharmacol Sci *92*, 19-27.
656 Xie, T., Peng, W., Yan, C., Wu, J., Gong, X., and Shi, Y. (2013). Structural insights into
657 RIP3-mediated necroptotic signaling. Cell Rep *5*, 70-78.
658 Yadav, V.K., Sudhagar, R.R., and Medhamurthy, R. (2002). Apoptosis during spontaneous
659 and prostaglandin F(2alpha)-induced luteal regression in the buffalo cow (Bubalus
660 bubalis): involvement of mitogen-activated protein kinases. Biol Reprod *67*, 752-759.
661 Ying, Z., Pan, C., Shao, T., Liu, L., Li, L., Guo, D., Zhang, S., Yuan, T., Cao, R., Jiang, Z.,
662 *et al.* (2018). Mixed Lineage Kinase Domain-like Protein MLKL Breaks Down Myelin
663 following Nerve Injury. Mol Cell *72*, 457-468 e455.
664 Zhang, D.W., Shao, J., Lin, J., Zhang, N., Lu, B.J., Lin, S.C., Dong, M.Q., and Han, J.
665 (2009). RIP3, an energy metabolism regulator that switches TNF-induced cell death from
666 apoptosis to necrosis. Science *325*, 332-336.
667 Zhang, T., Yin, C., Boyd, D.F., Quarato, G., Ingram, J.P., Shubina, M., Ragan, K.B.,
668 Ishizuka, T., Crawford, J.C., Tummers, B., *et al.* (2020). Influenza Virus Z-RNAs Induce
669 ZBP1-Mediated Necroptosis. Cell *180*, 1115-1129 e1113.
670 Zhang, X., Fan, C., Zhang, H., Zhao, Q., Liu, Y., Xu, C., Xie, Q., Wu, X., Yu, X., Zhang,
671 J., *et al.* (2016). MLKL and FADD Are Critical for Suppressing Progressive
672 Lymphoproliferative Disease and Activating the NLRP3 Inflammasome. Cell Rep *16*,
673 3247-3259.
674
675

676

677

678

679

680 **Figure legend**

681 **Figure 1.** RIPK3-induced apoptosis in MCF7 and KGN cells.

682 (**A**) Cultured MCF7/TO-RIPK3 and HeLa/TO-RIPK3 cells were treated with DMSO or
683 Dox(1μg/ml) induction for 36 hours. Cell viability was determined by measuring cellular
684 ATP levels (upper panel). The data are represented as the mean ± SD of triplicate wells.
685 The cell lysates were analyzed by western blotting using antibodies against RIPK3 or
686 β-actin (lower panel).

687 (**B**) Cultured MCF7/TO-RIPK3, KGN/TO-RIPK3, and HeLa/TO-RIPK3 cells were
688 treated with DMSO, Dox, or Dox plus TSZ for 36 hours. Cell viability was determined by
689 measuring cellular ATP levels. The data are represented as the mean ± SD of triplicate
690 wells.

691 (**C**) Cultured MCF7/TO-RIPK3 cells were treated with DMSO or Dox, plus the indicated
692 agents for 36 hours. Cell viability was determined by measuring cellular ATP levels (upper
693 panel). The data are represented as the mean ± SD of triplicate wells. The cell lysates were
694 analyzed by western blotting using antibodies against RIPK3 or β-actin (lower panel). 20
695 μM Z, pan-caspase inhibitor z-VAD; 2 μM RIPA-56, RIPK1 inhibitor; 2 μM NSA, MLKL
696 inhibitor.

697 (**D**) Cultured MCF7 cells were infected with lentiviruses encoding RIPK3(WT),
698 RIPK3(AAAA), RIPK3(K50A), and RIPK3(K50A)+GSK'872 plus Z for 36 hours. Cell
699 viability was determined by measuring cellular ATP levels (upper panel). The data are

represented as the mean ± SD of triplicate wells. ***$P<0.001$. The lysates were measured by western blotting using antibodies against RIPK3 or β-actin as indicated (lower panel). GSK'872, RIPK3 inhibitor.

The online version of this article includes the following figure supplement(s) for figure 1:

Figure supplement 1. RIPK3-induced apoptosis in human granulosa lutein cells (KGN).

Figure 2. RIPK3-induced apoptosis was dependent on RIPK1, FADD and caspase-8.

(**A**) Cultured MCF7/TO-RIPK3 cells were treated with DMSO or Dox plus the indicated agent for 24 hours. The cells were then harvested, and RIPK3 was immunoprecipitated from the cell lysates using anti-Flag resin. The cell lysates and immunocomplexes were analyzed by western blotting using antibodies as indicated.

(**B**-**E**) Cultured MCF7/TO-RIPK3(wild type (WT), *RIPK1*$^{-/-}$, *Caspase8*$^{-/-}$, *FADD*$^{-/-}$, and *cFLIF*$^{-/-}$) cells were treated with DMSO or Dox induction for 36 hours. Cell viability was determined by measuring cellular ATP levels (upper panel). The data are represented as the mean ± SD of triplicate wells. The cell lysates were analyzed by western blotting using antibodies against RIPK1, Caspase8, FADD, cFLIP or β-actin (lower panel).

Figure 3. RIPK3-mediated apoptosis is dependent on the auto-phosphorylation of the S164/T165 sites.

(**A**) Cultured MCF7/TO-RIPK3 and HeLa/TO-RIPK3 cells were treated with Dox plus z-VAD for 24 hours. RIPK3 was immunoprecipitated from the cell lysates using anti-Flag resin. The RIPK3 bands were excised and subjected to mass spectrometry analysis. RIPK3 specific phosphorylation site in MCF7/TO-RIPK3 cells is highlighted in red.

(**B**) Cultured KGN/TO-RIPK3, MCF7/TO-RIPK3, and HeLa/TO-RIPK3 cells were treated with Dox plus z-VAD for 24 hours. The lysates were analyzed by western blotting

using antibodies against the phopho-Serine164/theronine165 of RIPK3, Flag (RIPK3), and β-actin as indicated.

(**C**) Cultured MCF7 stably transfected with either wild type RIPK3 (WT) or kinase-dead mutant (D160N) cells under the control of Dox-inducible promoter were treated with DMSO(-) or Dox plus z-VAD for 24 hours. The lysates were analyzed by western blotting using antibodies against the phopho-Serine164/theronine165 RIPK3, Flag (RIPK3), and β-actin as indicated.

(**D**) Cultured 293T cells were transfected with Vector (Vec), RIPK3(WT), RIPK3(D160N), RIPK3(AAAA) (RIPK3-AAAA, residues 459-462 mutated to AAAA) and RIPK3(S164D/T165E) for 24 hours. The level of phospho-S227-RIPK3 and RIPK3 were measured by western blotting.

(**E** and **F**) Cultured MCF7 (E) and KGN (F) cells were infected with lentiviruses encoding RIPK3(WT), RIPK3(S164D/T165E), RIPK3(S164A/T165A) and RIPK3(AAAA) plus z-VAD for 36 hours. Cell viability was determined by measuring cellular ATP levels (upper panel). The data are represented as the mean ± SD of triplicate wells. ***$P<0.001$. The lysates were measured by western blotting using antibodies against RIPK3 or β-actin as indicated (lower panel).

(**G**) Cultured HeLa cells were infected with lentiviruses encoding RIPK3(WT), RIPK3(D160N), RIPK3(AAAA), and RIPK3(S164D/T165E) plus z-VAD for 36 hours. Cell viability was determined by measuring cellular ATP levels (upper panel). The data are represented as the mean ± SD of triplicate wells. **$P<0.01$, ***$P<0.001$. The expressed RIPK3 in the cell lysates were measured by western blotting using antibodies against RIPK3 or β-actin as indicated (lower panel). Vector (Vec, control viruses)

(**H**) Cultured HeLa cells were transfected with Flag-tagged RIPK3(WT), RIPK3(D160N), and RIPK3(S164D/T165E) for 24 hours. RIPK3 was immunoprecipitated using anti-Flag

resin. The lysates and immunocomplexes were analyzed by western blotting using antibodies against RIPK1, Caspase-8, FADD, and RIPK3 as indicated.

(**I**) Cultured MCF7/TO-RIPK3 and MCF7/TO-RIPK3(S164A/T165A) cells were treated with Dox plus Z for 24 hours. The cells were then harvested, and RIPK3 was immunoprecipitated from the cell lysates using anti-Flag resin. The cell lysates and immunocomplexes were analyzed by western blotting using antibodies as indicated.

The online version of this article includes the following figure supplement(s) for figure 3:

Figure supplement 1. Characterization of RIPK3 auto-phosphorylation sites.

Figure supplement 2. The phosphorylation site of RIPK3 is conserved among different mammalian species.

Figure 4. Hsp90/CDC37 chaperone determined the apoptotic and necroptotic function of RIPK3 kinase.

(**A**) The cell lysates from cultured HT29, HeLa, MCF7, and KGN cells were analyzed by western blotting using antibodies as indicated.

(**B** and **C**) Cultured HeLa-RIPK3, MCF7/TO-RIPK3, and KGN/TO-RIPK3 cells were treated with the indicated stimuli for 36 hours. Cell viability was determined by measuring cellular ATP levels. The data represented as the mean ± SD of triplicate wells. 17AAG, Hsp90 inhibitor.

(**D** and **E**) HeLa/TO-RIPK3 cells were treated with the indicated stimuli for 36 hours. Cell viability was determined by measuring cellular ATP levels in (D). The data represented as the mean ± SD of triplicate wells. ***$P<0.001$. 24 hours after treatment, the cell lysates were analyzed by western blotting using antibodies against phopho-Serine164/Theronine165 of RIPK3, RIPK3, and β-actin as indicated in (E).

(**F** and **G**) Cultured MCF7/TO-RIPK3 cells co-transfected with HSP90 and CDC37 as indicated were treated with DMSO or Dox for 36 hours. Cell viability was determined by measuring cellular ATP levels in (F). The data are represented as the mean ± SD of triplicate wells. ***$P<0.001$. 24 hours after treatment, the cell lysates were analyzed by western blotting using antibodies against phopho-Serine164/Theronine165 of RIPK3, RIPK3, Hsp90, CDC37, and β-actin as indicated in (G).

(**H**) Cultured HeLa/TO-RIPK3 cells were treated with Dox or Dox plus 17AAG for 24 hours. The cells were then harvested, and RIPK3 was immunoprecipitated from the cell lysates using anti-Flag resin. The cell lysates and immunocomplexes were analyzed by western blotting using antibodies as indicated.

(**I**) Cultured HeLa/TO-RIPK3 cells were treated with Dox or Dox plus 17AAG for 24 hours. Immunofluorescence of the cells with Flag-RIPK3 (red) antibody. Counterstaining with DAPI (blue). Scale bar, 10 μm. Higher-power views (right panels) were acquired from the selected boxed areas from the left panel.

(**J**) Cultured MCF7/TO-RIPK3 cells co-transfected with HSP90 and CDC37 as indicated were treated with Dox for 24 hours. Immunofluorescence of the cells with Flag-RIPK3 (red) antibody. Counterstaining with DAPI (blue). Scale bar, 10 μm. Higher-power views (right panels) were acquired from the selected boxed areas from the left panel.

The online version of this article includes the following figure supplement(s) for figure 4:

Figure supplement 1. Hsp90/CDC37 chaperone determines the necroptotic or apoptotic function of RIPK3 kinase.

Figure supplement 2. RIPK3 form amyloid-like structure in MCF7 and KGN cells.

Figure supplement 3. Hsp90/CDC37 chaperone protein levels was low in corpus luteum and corpus albicans.

Figure 5. *Ripk3*$^{S165D\text{-}T166D/S165D\text{-}T166D}$ (*Ripk3*$^{ST\text{-}DE/ST\text{-}DE}$) mice die within one month after birth.

(**A** and **B**) Macroscopic features (A) and body weights (B) of *Ripk3*$^{+/+}$ and *Ripk3*$^{ST\text{-}DE/ST\text{-}DE}$ littermate mice at 14 days of age (n≥9). The result from each individual animal is presented as an indicated dot. ***$P<0.001$.

(**C**) Kaplan-Meier plot of survival of *Ripk3*$^{+/+}$ and *Ripk3*$^{ST\text{-}DE/ST\text{-}DE}$ littermate mice (n=10 for each genotype) after birth within two months. ***$P<0.001$.

(**D**) Histological analysis of large intestine, small intestine, lung, and spleen of *Ripk3*$^{+/+}$ and *Ripk3*$^{ST\text{-}DE/ST\text{-}DE}$ littermate mice (n=5) at 14 days of age. Scale bar, 20 μm.

(**E** and **F**) Representative immunohistochemistry (IHC) images of the large intestine, small intestine, lung, and spleen of *Ripk3*$^{+/+}$ and *Ripk3*$^{ST\text{-}DE/ST\text{-}DE}$ littermate mice (n=5, 14 days) stained with a Cleaved-Caspase3 (C-C3) antibody in (E). C-C3 positive cells were counted in two fields per organ and quantified in (F). Scale bar, 10 μm. Data represent the mean ± s.e.m. **$P<0.01$, ***$P<0.001$.

(**G**) Cell viability measurement of bone marrow-derived macrophages from the *Ripk3*$^{+/+}$ and *Ripk3*$^{ST\text{-}DE/ST\text{-}DE}$ littermate mice (n=3, 14 days) after treatment with the indicated Z-VAD or necroptosis stimuli for 24 hours. Cell viability was determined by measuring cellular ATP levels. The data are represented as the mean ± SD of triplicate wells.

The online version of this article includes the following figure supplement(s) for figure 5:

Figure supplement 1. Generation of *Ripk3*$^{ST\text{-}DE/ST\text{-}DE}$ and *Ripk3*$^{ST\text{-}AA/ST\text{-}AA}$ mice.

Figure 6. Phospho-serine164/threonine165-RIPK3 signals were present in aged ovary corpus albican.

(**A**) Western blot analysis of RIPK1, RIPK3, and MLKL levels in perfused mouse ovary extracts of different ages. Each group is representative of at least 3 mice.

(**B**) H&E and immunofluorescence (IF) imaging of an 8-month-old ovary. Two adjacent sections were analyzed. One section was stained with H&E, and the other was IF stained with a RIPK3 antibody (red) and DAPI (blue). Scale bar, 500 μm. Higher-power views of selected areas were acquired in **a** (primordia follicle), **b** (secondary follicle), **c** (corpus luteum), and **d** (corpus albicans) as indicated. PF, primary follicle; CL, corpus luteum; CA, corpus albicans.

(**C**) Ovarian $PGF_{2\alpha}$ levels of wild-type mice (n=8) at the indicated age assayed by ELISA. Data represent the mean ± s.e.m. $^{**}P<0.01$, $^{***}P<0.001$.

(**D**) Immunofluorescence images of a RIPK3 C-terminus HA-3×Flag knock-in mouse ovary (n=5; 12 months) stained with antibodies against prostaglandin F receptor (PTGFR, green) and Flag (red). Counterstaining with DAPI (blue). Scale bar, 500 μm. Higher-power views (right panels) were acquired from the indicated boxed area in the second lower left panel. CL, corpus luteum. CA, corpus albicans. Scale bar, 100 μm.

(**E**) Western blot analysis of p-S164/T165-RIPK3 and RIPK3 levels in extracts from perfused ovaries prepared from mice at the indicated age. Each group is representative of at least 3 mice.

(**F**) Immunofluorescence images of ovaries from *Ripk3*$^{+/+}$ and *Ripk3*$^{-/-}$ mice (4 Month, 8 Month and 12 Month; n=3) at the indicated ages stained with the p-S164/T165-RIPK3 antibody (red). Counterstaining with DAPI (blue). Scale bar, 200 μm. Higher-power views (lower two panels) were acquired from the selected boxed areas from the upper panel. (CL), b (CL), c (CL, CA) and d (CL). F, follicle; CL, corpus luteum; CA, corpus albicans. Scale bar, 100 μm.

The online version of this article includes the following figure supplement(s) for figure 6:

Figure supplement 1. Generation of RIPK3 C-terminus HA-3×Flag knock-in and *Ptgfr*$^{-/-}$ mice.

Figure 7. Prostaglandin F2alpha ($PGF_{2\alpha}$) induces ovarian RIPK3 expression for corpus luteum involution.

(**A** to **C**) Primary granulosal lutein cells (WT, *Ripk3*$^{-/-}$) were isolated from 3-month-old mice ovaries. The cells were treated with Dinoprost Tromethamine (DT) at the indicated concentration for 36 hours in (A); with 1.5 μM DT at the indicated time in (B); or with 1.5 μM DT for 36 hours in (C). The cell lysates from the DT-treated cells were analyzed by western blotting using antibodies as indicated.

(**D** and **E**) *Ptgfr*$^{+/+}$ and *Ptgfr*$^{-/-}$ littermate female mice (n=16; 25-26 days) were given 7.5 IU pregnant mare serum gonadotropin (PMSG) intraperitoneally(IP) followed by 7.5 IU serum gonadotropin and chorionic gonadotropin (SCG) 46 hours later to synchronize ovulation. The animals were then injected with Dinoprost Tromethamine (DT) (10 micrograms, i.p.) or saline 24 hours post-ovulation. Ovaries were then collected 12 hours later and stained with anti-RIPK3 antibody (red) in (D). The ovary lysates were analyzed by western blotting using antibodies as indicated in (E). (*) indicates Corpus luteum. Counterstaining with DAPI (blue). Scale bar, 500 μm.

(**F** and **G**) wild type(WT), *Ripk3*$^{-/-}$, *Ripk3*$^{S165A\text{-}T166A/S165A\text{-}T166A}$, *Fadd*$^{-/-}$*Mlkl*$^{-/-}$ and *Ptgfr*$^{-/-}$ female mice (each group, n=16; 25-26 days) were treated as in (D and F). Ovaries from each group were then collected 24 hours after injecting with DT and stained with anti-cleaved-caspase3 antibody in (F). The Cleaved-Caspase3^{+} cells were counted in five fields per ovary Corpus luteum(CL) and quantified in (G). Scale bar, 20 μm. Data represent the mean ± s.e.m. $^{**}P<0.01$, $^{***}P<0.001$.

(**H**) wild type female mice (n=3; 25-26 days) were treated as in (D and F). Ovaries were then collected 12 hours after injecting with DT and stained with anti-cleaved-caspase3(red)

and p-S164/T165-RIPK3(green) antibody. Counterstaining with DAPI (blue). Scale bar, 100 μm.

The online version of this article includes the following figure supplement(s) for figure 7:

Figure supplement 1. Prostaglandin F2alpha ($PGF_{2\alpha}$) stimulates RIPK3 expression through the MAPK pathway.

Figure supplement legend

Figure 1-figure supplement 1. RIPK3-induced apoptosis in human granulosa lutein cells (KGN).

Cultured KGN/TO-RIPK3 cells were treated with DMSO or Dox(1μg/ml) induction for 36 hours. Cell viability was determined by measuring cellular ATP levels (upper panel). The data are represented as the mean ± SD of triplicate wells. The cell lysates were analyzed by western blotting using antibodies against RIPK3 or β-actin (lower panel).

Figure 3-figure supplement 1. Characterization of RIPK3 auto-phosphorylation sites.

(**A**) Cultured MCF7/TO-RIPK3 and MCF7/TO-RIPK3(S164A/T165A) cells were treated with DMSO (-) or Dox plus z-VAD for 24 hours. The lysates were analyzed by western blotting using antibodies against the phopho-Serine164/theronine165 of RIPK3, Flag (RIPK3), and β-actin as indicated.

(**B**) Cultured KGN7/TO-RIPK3 and KGN/TO-RIPK3(S164A/T165A) cells were treated with DMSO or Dox plus z-VAD for 24 hours. The lysates were analyzed by western blotting using antibodies against the phopho-Serine164/theronine165 of RIPK3, Flag (RIPK3), and β-actin as indicated.

(**C**) Cultured MCF7/TO-RIPK3 and MCF7/TO-RIPK3(K50A) cells were treated with DMSO (-) or Dox plus z-VAD for 24 hours. The lysates were analyzed by western blotting using antibodies against the phopho-Serine164/theronine165 of RIPK3, Flag (RIPK3), and β-actin as indicated.

(**D**) Cultured HeLa cells were infected with lentiviruses encoding wild type RIPK3(WT), and mutant RIPK3 including RIPK3(D160N), RIPK3(S164D/T165E), RIPK3(S164E), RIPK3(T165E), RIPK3(S164A/T165A), RIPK3(S164A), RIPK3(T165A) and RIPK3(AAAA) and treated with TSZ for 36 hours. Cell viability was determined by measuring cellular ATP levels (upper panel). The data represented as the mean ± SD of triplicate wells. $^{**}P < 0.01$. The levels of expressed RIPK3 in the cell lysates were measured by western blotting (lower panel).

(**E**) RIPK3 single site (S164E) mutation blocks auto-phosphorylation. 293T cells were transfected with Flag-tagged RIPK3(WT), RIPK3(D160N), RIPK3(S164D/T165E), RIPK3(S164E), RIPK3(T165E), RIPK3(S164A/T165A), RIPK3(S164A), RIPK3(T165A) and RIPK3(AAAA) for 24 hours. The level of p-S227-RIPK3 and RIPK3 were measured by western blotting.

(**F** and **G**) Cultured MCF7 (E) and KGN (F) cells were infected with lentiviruses encoding wild type RIPK3(WT), and mutant forms of RIPK3(S164A/T165A), RIPK3(S164A) and RIPK3(T165A) and treated with z-VAD as indicated for 36 hours. Cell viability was determined by measuring cellular ATP levels (upper panel). The data are represented as the mean ± SD of triplicate wells. $^{***}P < 0.001$. The levels of RIPK3 in the cell lysates were measured by western blotting (lower panel).

(**H**) Cultured HeLa cells were transfected with Flag-tagged wild type RIPK3(WT), and mutant forms of RIPK3(T165E), RIPK3(S164D/T165E), and RIPK3(S164E) for 24 hours. RIPK3 was immunoprecipitated from the cell lysates using anti-Flag resin. The

922 lysates and immunocomplexes were analyzed by western blotting using antibodies against
923 RIPK1, caspase-8, RIPK3, and β-actin as indicated.
924
925 **Figure 3-figure supplement 2.** The phosphorylation site of RIPK3 is conserved among
926 different mammalian species.
927 (**A**) Alignment of amino acid sequences of RIPK3 orthologs in five mammalian species.
928 Amino acid residues conserved in 80% or more of the sequences are shaded in black. The
929 putative phosphorylation residues are denoted by asterisks (*).
930 (**B**) Cultured 293T cells were transfected with Vector (Vec), mouse RIPK3(WT),
931 RIPK3(S165D/T166E), and RIPK3(S165A/T165A) for 24 hours. The level of
932 phospho-S232-RIPK3 and RIPK3 were measured by western blotting.
933 (**C**) Cultured mouse sarcoma cells L929(*Ripk3*$^{-/-}$) were transfected with Vector, wild type
934 mouse RIPK3, and mutant forms of mRIPK3(D161N), and mRIPK3(S165D/T166E) and
935 treated with z-VAD or TSZ as indicated for 36 hours. Cell viability was determined by
936 measuring cellular ATP levels (upper panel). The data represented as the mean ± SD of
937 triplicate wells. The lysates were analyzed by western blotting using antibodies as
938 indicated (lower panel).
939
940 **Figure 4-figure supplement 1.** Hsp90/CDC37 chaperone determines the necroptotic or
941 apoptotic function of RIPK3 kinase.
942 (**A**) HeLa/TO-RIPK3 and HeLa/TO-RIPK3-shRNA-HSP90 cells were treated with the
943 indicated stimuli for 36 hours. Cell viability was determined by measuring cellular ATP
944 levels. The data represented as the mean ± SD of triplicate wells. ***$P<0.001$. The cell
945 lysates were analyzed by western blotting using antibodies as indicated (right panel).

(**B**) L929 cells were treated with the indicated stimuli for 5 hours. Cell viability was determined by measuring cellular ATP levels. The data represented as the mean ± SD of triplicate wells.

(**C**) L929(*Ripk3*$^{-/-}$)/TO-RIPK3 and L929(*Ripk3*$^{-/-}$)/TO-RIPK3-shRNA-HSP90 cells were treated with the indicated stimuli for 36 hours. Cell viability was determined by measuring cellular ATP levels. The data represented as the mean ± SD of triplicate wells. ***$P<$ 0.001. The cell lysates were analyzed by western blotting using antibodies as indicated (right panel).

(**D** and **E**) L929(*Ripk3*$^{-/-}$)/TO-RIPK3 cells were treated with the indicated stimuli for 36 hours. Cell viability was determined by measuring cellular ATP levels in (D). The data represented as the mean ± SD of triplicate wells. **$P<0.01$, ***$P<0.001$. 24 hours after treatment, the cell lysates were analyzed by western blotting using antibodies against phopho-Serine165/Theronine166 of RIPK3, RIPK3, and β-actin as indicated in (E).

Figure 4-figure supplement 2. RIPK3 form amyloid-like structure in MCF7 and KGN cells.

(**A**) Cultured HeLa/TO-RIPK3 and MCF7/TO-RIPK3 cells were treated with DMSO or Dox plus TSZ for 24 hours. Immunofluorescence of the cells with Flag-RIPK3 (green) antibody. Counterstaining with DAPI (blue). Scale bar, 10 μm. Higher-power views (right panels) were acquired from the selected boxed areas from the left panel.

(**B**) Cultured HT29 and KGN/TO-RIPK3 cells were treated with DMSO, TSZ, or Dox for 24 hours. Immunofluorescence of the cells with Flag-RIPK3 (green) antibody. Counterstaining with DAPI (blue). Scale bar, 10 μm. Higher-power views (right panels) were acquired from the selected boxed areas from the left panel.

(**C**) Cultured HeLa/TO-RIPK3 and MCF7/TO-RIPK3 cells were treated with Dox plus Z for 24 hours. Immunofluorescence of the cells with Flag-RIPK3 (red) and p-S164/T165-RIPK3(green) antibody. Counterstaining with DAPI (blue). Scale bar, 10 μm. Higher-power views (right panels) were acquired from the selected boxed areas from the left panel.

(**D**) Cultured MCF7/TO-RIPK3(WT, *RIPK1*$^{-/-}$, *caspase-8*$^{-/-}$ and *FADD*$^{-/-}$) cells were treated with Dox plus Z for 24 hours. Immunofluorescence of the cells with Flag-RIPK3 (red) and p-S164/T165-RIPK3(green) antibody. Counterstaining with DAPI (blue). Scale bar, 10 μm. Higher-power views (right panels) were acquired from the selected boxed areas from the left panel.

(**E**) Cultured MCF7/TO-RIPK3(WT, *RIPK1*$^{-/-}$, *caspase-8*$^{-/-}$ and *FADD*$^{-/-}$) cells were treated with DMSO or Dox plus Z for 24 hours. The lysates were analyzed by western blotting using antibodies as indicated.

Figure 4-figure supplement 3. Hsp90/CDC37 chaperone protein levels was low in corpus luteum and corpus albicans.

(**A** and **B**) Immunofluorescence of ovary from wild type mice (8 Month; n=3) with RIPK3 (red) and HSP90 (green) antibody in (A). Higher-power views of selected areas were acquired in right panel. The HSP90/RIPK3 levels were quantified in (B). F, follicle. CA, corpus albicans. Scale bar, 100/200 μm.

(**C** and **D**) Immunofluorescence of ovary from wild type mice (8 Month; n=3) with RIPK3 (red) and CDC37 (green) antibody in (C). Higher-power views of selected areas were acquired in right panel. The CDC37/RIPK3 levels were quantified in (D). F, follicle. CA, corpus albicans. Scale bar, 200 μm.

Figure 5-figure supplement 1. Generation of *Ripk3*$^{ST\text{-}DE/ST\text{-}DE}$ and *Ripk3*$^{ST\text{-}AA/ST\text{-}AA}$ mice.

(**A**) Two guide RNA and donate oligo sequences of *Ripk3(S165D/T166E)* and *Ripk3(S165A/T166A)* knock-in mice.

(**B**) Schematic of CRISPER-Cas9 strategy for the generation for *Ripk3(S165D/T166E)* and *Ripk3(S165A/T166A)* knock-in mice. The gene structure of RIPK3 and two guide RNA sequences targeting the exon 4 of RIPK3 were shown with the PAM sequences highlighted in red and blue.

(**C** and **D**) Macroscopic features (C) and body weights (D) of *Ripk3*$^{+/+}$ and *Ripk3*$^{ST\text{-}AA/ST\text{-}AA}$ littermate mice at 14 days of age (n=10). The result from each individual animal was presented as an indicated dot. NS, not significant.

(**E** and **F**) Immunoblot of RIPK3 from lung extracts of 14 days old *Ripk3*$^{+/+}$, *Ripk3*$^{ST\text{-}DE/ST\text{-}DE}$, and *Ripk3*$^{ST\text{-}AA/ST\text{-}AA}$ littermates using antibodies against RIPK3 and GAPDH as indicated (n=3).

(**G**) Histological analysis of brain, cerebellum, heart, kidney, and liver of *Ripk3*$^{+/+}$ and *Ripk3*$^{ST\text{-}DE/ST\text{-}DE}$ littermate mice (n=5) at 14 days of age. Scale bar, 20 μm. PTC, Proximal tubular cell.

(**H**) Cell viability measurement of bone marrow-derived macrophages from the *Ripk3*$^{+/+}$ and *Ripk3*$^{ST\text{-}AA/ST\text{-}AA}$ littermate mice (n=3, 14 days) after treatment with the indicated necroptosis stimuli for 24 hours. Cell viability was determined by measuring cellular ATP levels. The data represented as the mean ± SD of triplicate wells.

Figure 6-figure supplement 1. Generation of RIPK3 C-terminus HA-3×Flag knock-in and *Ptgfr*$^{-/-}$ mice.

(**A**) Schematic of CRISPER-Cas9 strategy for RIPK3 C-terminus HA-3×Flag knock-in mice. The gene structure of RIPK3 and guide RNA sequences targeting the *Ripk3* were shown with the PAM sequences highlighted in red.

(**B**) Western blotting analysis using protein extracts from the ovary of wild type, heterozygous knock-in, and homozygous knock-in mice generated as illustrated in (A).

(**C**) Schematic of CRISPER-Cas9 strategy for the generation for $Ptgfr^{-/-}$ mice. The gene structure of PTGFR and two guide RNA sequences targeting the *Ptgfr* were shown with the PAM sequences highlighted in red.

(**D**) Immunoblot of PTGFR from ovary extracts of 2-month old $Ptgfr^{+/+}$ and $Ptgfr^{-/-}$ littermates using antibodies against PTGFR and GAPDH as indicated (n=3).

Figure 7-figure supplement 1. Prostaglandin F2alpha ($PGF_{2\alpha}$) stimulates RIPK3 expression through the MAPK pathway.

(**A**) Primary granulosal lutein cells were isolated from the 3-month-old mice ovary. The cells were then treated with 1 μM DT or plus MAPK inhibitors PD-98059 (5 μM) and U0126 (5 μM) as indicated for 36 hours. The lysates were analyzed by western blotting using antibodies as indicated.

(**B**) Primary granulosal lutein cells were isolated from 3-month-old mice ovaries. The cells were treated with 1 μM DT at the indicated time. The cell lysates from the DT-treated cells were analyzed by western blotting using antibodies as indicated.

(**C**) Diagram of induction of corpus luteum regression *in vivo*.

(**D**) $Ripk3^{+/+}$ and $Ripk3^{S165A\text{-}T166A/S165A\text{-}T166A}$ and littermate female mice (n=3; 25-26 days) were given 7.5 IU pregnant mare serum gonadotropin (PMSG) intraperitoneally(IP) followed by 7.5 IU serum gonadotropin and chorionic gonadotropin (SCG) 46 hours later to synchronize ovulation. The animals were then injected with Dinoprost Tromethamine

(DT) (10 micrograms, i.p.) or saline 24 hours post-ovulation. The ovary lysates were analyzed by western blotting using antibodies as indicated.

Materials and methods

Animals

The *Ripk3*$^{-/-}$ and *Mlkl*$^{-/-}$ mice (C57BL/6J strain) have been described previously (He et al., 2009; Ying et al., 2018). *Fadd*$^{+/-}$*Mlkl*$^{-/-}$ mice were provided by Dr. Haibing Zhang (Institute for Nutritional Sciences, Shanghai, China) (Zhang et al., 2016). C57BL/6J wild type (WT) mice were obtained from Vital River Laboratory Co. WT, *Ripk3*$^{-/-}$, *Mlkl*$^{-/-}$ and *Fadd*$^{-/-}$*Mlkl*$^{-/-}$ mice were produced and maintained at the SPF animal facility of the National Institute of Biological Sciences, Beijing. Animals for the aging study were produced by mating wild type males with wild type females purchased from Vital River Laboratory Co; *Ripk3*$^{-/-}$ mice were produced by mating *Ripk3*$^{-/-}$ males with *Ripk3*$^{-/-}$ females. *Fadd*$^{-/-}$*Mlkl*$^{-/-}$ mice were produced by mating *Fadd*$^{+/-}$*Mlkl*$^{-/-}$ males with *Fadd*$^{+/-}$*Mlkl*$^{-/-}$ females. *Ripk3*$^{S165D\text{-}T166E/\ S165D\text{-}T166E}$ and *Ripk3*$^{S165A\text{-}T166A/\ S165A\text{-}T166A}$ knock-in mice were generated using the CRISPR-Cas9 system (Figure 5-figure supplement 1). The *Ripk3* C terminus HA-3xFlag knock-in and *Ptgfr* knockout mice were generated using the CRISPR-Cas9 system (Figure 6-figure supplement 1).

The primers used for genotyping are listed below:

Ripk3-(WT)-F: 5’-GCTAGCAGATTTTGGCCTGTCCACG-3’;

Ripk3-(S165D/T166E)-F: 5’-GCTAGCAGATTTTGGCCTGGACGAA-3’;

Ripk3-(S165A/T166A)-F: 5’-GCTAGCAGATTTTGGCCTGGCAGCA-3’;

Ripk3-R: 5’-GGCCTCTGGCGAGACTTCTTTCCTG-3’;

Ptgfr-WT-F: 5’-GCTGTGTTAGCCCATTGAGTCAGGTAGA-3’;

Ptgfr-KO-F: 5’-TGATGGTGTCAGTTTGGGCGGTAT-3’;

Ptgfr-KO-R: 5'-GCTTTACTTCTGCTACTGAATTCCCTTGG-3';

Mouse husbandry

Mice were group-housed in a 12 hours light/dark (light between 08:00 and 20:00) in a temperature-controlled room (21.1 ± 1 °C) at the National Institute of Biological Sciences with free access to water. The ages of mice are indicated in the figure, figure legends, or methods. All animal experiments were conducted following the Ministry of Health national guidelines for the housing and care of laboratory animals and were performed in accordance with institutional regulations after review and approval by the Institutional Animal Care and Use Committee at the National Institute of Biological Sciences, Beijing.

Antibodies and reagents

Antibodies for mouse RIPK3 (#2283; WB, 1:1000; IHC, 1:100) were obtained from ProSci. There other antibodies used in this study were anti-RIPK3(LS-C336804, LSBio; WB, 1:1000; IHC 1:100), anti-GAPDH-HRP (M171-1, MBL; WB, 1:5000), anti-β-Actin-HRP (PM053-7, MBL; WB, 1:5000), anti-Tubulin-HRP (PM054-7, MBL; WB, 1:5000), anti-RIPK1 (#3493S, Cell Signaling; WB, 1:2000), anti-Human-MLKL (ab184718, abcam; WB, 1:2000), anti-Mouse-MLKL (AO14272B, ABGENT; WB, 1:2000), anti-Caspase8 (#9746, Cell Signaling; WB, 1:1000), anti-FADD (#2782, Cell Signaling; WB, 1:1000), anti-cFLIP (ab6144, Abcam; WB, 1:1000),anti-Cleaved-Caspase3 (#9661, Cell Signaling; WB, 1:1000; IHC, 1:100), anti-Cleaved-Caspase3 (STJ97448, St John's Laboratory; IHC, 1:100), anti-Cleaved-Caspase3 (ab2302, abcam; WB, 1:1000), anti-Human-p-S227-RIPK3(ab209384, abcam; WB, 1:1000), anti-Flag-HRP (A8592, Sigma-Aldrich; WB, 1:5000), anti-Prostaglandin F2 alpha(PTGFR) (ab203342, abcam;

IHC, 1:100), anti-HSP90 (13171-1-AP, proteintech; WB, 1:1000; IHC, 1:100), anti-CDC37 (B109419, abcam; WB, 1:1000; IHC, 1:100), anti-FLAG® M2 (F1840, Sigma-Aldrich; IHC, 1:100), anti-Phospho-p44/42 MAPK (4370S, Cell Signaling; WB, 1:1000), anti-p44/42 MAPK (4965S, Cell Signaling; WB, 1:1000), anti-Phospho-MEK1/2 (9154S, Cell Signaling; WB, 1:1000), anti-MEK1/2 (ab178876, abcam; WB, 1:1000). Donkey anti-Mouse, Alexa Fluor 488 (Thermo Fisher, A-21202), Donkey anti-Mouse, Alexa Fluor 555 (Thermo Fisher, A-31570), Donkey anti-Rabbit, Alexa Fluor 488 (Thermo Fisher, A-21206), Donkey anti-Rabbit, Alexa Fluor 555 (Thermo Fisher, A-31572). Dinoprost Tromethamine(S5056), PD-98059(S1177) and U0126(S1102) were purchased from Selleck. pyridine-3-sulfonyl (PS) was purchased from Sigma. Pregnant Mare Serum Gonadotropin (PMSG)(110254564) and Gonadotropin and Serum chorionic Gonadotropin (SCG) (110251283) were purchased from Ningbo Second Hormone Factory.

We collaborated with Epitomics to develop the rabbit monoclonal antibody against p-S164/T165-RIPK3 (Abcam, Ab255705; WB, 1:1000; IHC, 1:100). The rabbits were immunized with the peptide. Hybridoma lines were screened by western blot analysis. The final antibody was purified using protein A agarose.

Cell lines and cell cultures

All cells were cultured at 37°C with 5% CO_2. All cell lines were cultured as follows: HT29 cells were obtained from ATCC and cultured in McCoy's 5A culture medium(Invitrogen). HEK293T, HeLa and MCF7 cells were obtained from ATCC and cultured in DMEM (Hyclone). L929(*Ripk3*$^{-/-}$) cells were cultured in DMEM (Hyclone) (Ying et al., 2018). Human granulosa tumor cell line (KGN) (Nishi et al., 2001), were kindly provided by Dr. Qiao Jie from Peking University Third Hospital in China and

were cultured in DMEM:F12 Medium (Hyclone). Stable KGN or MCF7 cell lines expressing the Tet repressor (KGN-Tet-On cells and MCF7-Tet-On cells) were selected with 1 mg/ml G418 after being infected with virus encoding Tet repressor. KGN-Tet-On and MCF7-Tet-On cells were infected with virus encoding 3×Flag-RIPK3 or another mutant and were selected with 10 μg/ml puromycin to establish the KGN/TO-RIPK3/RIPK3(S164A/T165A) and MCF7/TO-RIPK3/RIPK3(D160N)/RIPK3(S164A/T165A) cell lines. All media were supplemented with 10% FBS (Thermo Fisher) and 100 units/ml penicillin/ streptomycin (Thermo Fisher).

Plasmids constructs

Full-length human RIPK3, RIPK3(AAAA) (RIPK1 interaction mutant RIPK3, the residues 459-462 within RHIM region were mutated to four alanine residues) and mouse RIPK3 cDNA were kept in our lab and subcloned into the pWPI vector (GFP-tagged) to generate pWPI-HA-3×Flag-RIPK3/RIPK3(D160N)/RIPK3(AAAA) and pWPI-HA-3×Flag-mRIPK3 virus construct. Using Quickchange Site-Directed Mutagenesis Kit to generate pWPI-HA-3×Flag-RIPK3(D160N)/RIPK3(S164D/T165E)/RIPK3(S164E)/RIPK3(T165E)/RIPK3(S164A/T165A)/RIPK3(S164A)/RIPK3(T165A) and pWPI-HA-3×Flag-mRIPK3(D161N)/mRIPK3(S165D/T166E) virus construct.

pLVX-Tight-Puro Vector and pLVX-Tet-On Advanced were kindly provided by Dr. Wenhui Li lab at NIBS. Full-length human RIPK3 or RIPK3 mutant were subcloned into the pLVX-Tight-Puro Vector to generate pLVX-Tight-HA-3×Flag-RIPK3/RIPK3(D160N)/RIPK3(S164A/T165A) construct. The gRNAs for targeting *RIPK1*(5'-ATGCTCTTACCAGGAAATGT-3'),

Caspase-8(5'-TGATCGACCCTCCGCCAGAA-3'), *FADD*(5'-AGTCGTCGACGCGCCGCAGC-3') and *cFLIP*(5'-TACCAGACTGCTTGTACTTC-3') were designed and were cloned into the gRNA-Cas9 expression plasmid pX458-GFP to generate pX458-GFP-RIPK1/Caspase-8/FADD/cFLIP construct.

Cell survival assay

Cell survival assay was performed using Cell Titer-Glo Luminescent Cell Viability Assay kit. A Cell Titer-Glo assay (Promega, G7570) was performed according to the manufacturer's instructions. Luminescence was recorded with a Tecan GENios Pro plate reader.

Transfections

HeLa or HEK293T cells were transfected with plasmids using Lipofectamine 3000 (ThermoFisher Scientific) following the manufacturer's instructions.

Live-cell imaging

On day 1, KGN cells were plated in a 37°C imaging station chamber. On day 2, KGN cells were infected with viruses (Flag-RIPK3, GFP label) for 20 hours. Images were obtained with a Nikon Ti inverted microscope and the PerkinElmer UltraVIEW VoX system. Time-lapse images were captured at 3-min intervals using a Nikon PLAN APO 60× objective. The images were processed using Volocity software.

Virus packaging

To prepare the Virus, HEK293T cells in the 10-cm dish were transfected with 15 μg of pWPI Vector (Vec, control viruses), pWPI-HA-3×Flag-RIPK3/RIPK3(D160N)/RIPK3(AAAA)/ RIPK3(S164D/T165E) /RIPK3(S164E)/ RIPK3(T165E) /RIPK3(S164A/T165A)/RIPK3(S164A) /RIPK3(T165A), pLVX-Tight-3×Flag-RIPK3/RIPK3(D160N)/RIPK3(S164A/T165A) or pLVX-Tet-On Advanced DNA together with 11.25 μg of psPAX2 and 3.75 μg of pMD2.G Eight hours after transfection, the media were changed to high-serum DMEM (20% FBS with 25 mM HEPES). Another 40 hours later, the media were collected and centrifuged at 3,000 r.p.m. for 10 min. The supernatant was filtered through a 0.22-μm membrane, and aliquots of 15 ml were stored at -80 °C.

CRISPR/Cas9 knockout cells

4 μg of pX458-GFP-RIPK1/Caspase-8/FADD/cFLIP plasmid was transfected into 1×10^7 MCF7/TO-RIPK3 cells using the Transfection Reagent (FuGENE® HD, E2311) by following the manufacturer's instructions. 3 days after the transfection, GFP-positive live cells were sorted into single clones by using a BD FACSArial cell sorter. The single clones were cultured into 96-well plates for another 10-14 days or longer, depending upon the cell growth rate. The anti- RIPK1/Caspase-8/FADD/cFLIP immunoblotting was used to screen for the MCF7/TO-RIPK3 (*RIPK1*$^{-/-}$*/Caspase-8*$^{-/-}$*/FADD*$^{-/-}$*/cFLIP*$^{-/-}$) clones. Genome type of the knockout cells was determined by DNA sequencing.

Western blotting

Western blotting was performed as previously described. Cell pellet samples were collected and re-suspended in lysis buffer (100 mM Tris-HCl, pH 7.4, 100 mM NaCl, 10% glycerol, 1% Triton X-100, 2 mM EDTA, Roche complete protease inhibitor set,

and Sigma phosphatase inhibitor set), incubated on ice for 30 min, and centrifuged at 20,000 × g for 30 min. The supernatants were collected for western blotting. Ovary or other tissue were ground and re-suspended in lysis buffer, homogenized for 30 seconds with a Paddle Blender (Prima, PB100), incubated on ice for 30 min, and centrifuged at 20,000 × g for 30 min. The supernatants were collected for western blotting.

Immunoprecipitation

The cells were cultured on 10-cm dishes and grown to confluence. Cells at 70% confluence with or without Dox (1 μg/ml) induction for 24 hours. Then cells were washed once with PBS and harvested by scraping and centrifugation at 800 × g for 5 min. The harvested cells were washed with PBS and lysed for 30 min on ice in the lysis buffer. Cell lysates were then spun down at 12,000 × g for 20 min. The soluble fraction was collected, and the protein concentration was determined by Bradford assay. Cell extracted was mixed with anti-Flag affinity gel (Sigma-Aldrich, A2220) in a ratio of 1 mg of extract per 30 μl of agarose. After overnight rocking at 4 °C, the beads were washed 3 times with lysis buffer. The beads were then eluted with 0.5 mg/mL of the corresponding antigenic peptide for 6 hours or directly boiled in 1× SDS loading buffer (125 mM Tris, PH 6.8, 2% 2-mercaptoethanol, 3% SDS, 10% glycerol and 0.01% bromophenol blue).

Tissue collection

Mice were sacrificed and perfused with PBS. Tissues for stain comparisons were taken at the same stage of the estrous cycle: ovarian were taken from all mice during diestrus. Major organs were removed, cut into appropriately-sized pieces, and either flash-frozen in liquid nitrogen and stored at -80 °C or placed in 4% paraformaldehyde for

preservation. After several days of 4% paraformaldehyde fixation at room temperature, tissue fragments were transferred to 70% ethanol and stored at 4°C.

Histology and immunohistochemistry

Paraffin-embedded specimens were sectioned to a 5 μm thickness and were then deparaffinized, rehydrated, and stained with haematoxylin and eosin (H&E) using standard protocols. For the preparation of the immunohistochemistry samples, sections were dewaxed, incubated in boiling citrate buffer solution for 15 min in plastic dishes, and subsequently allowed to cool down to room temperature over 3 hours. Endogenous peroxidase activity was blocked by immersing the slides in Hydrogen peroxide buffer (10%, Sinopharm Chemical Reagent) for 15 min at room temperature and were then washed with PBS. Blocking buffer (1% bovine serum albumin in PBS) was added, and the slides were incubated for 2 hours at room temperature. Primary antibody against Flag, RIPK3, Cleaved-Caspase3, and p-S164/T165-RIPK3 was incubated overnight at 4°C in PBS. After 3 washes with PBS, slides were incubated with secondary antibody (polymer-horseradish-peroxidase-labeled anti-rabbit, Sigma) in PBS. After a further 3 washes, slides were analyzed using a diaminobutyric acid substrate kit (Thermo Fisher). Slides were counterstained with haematoxylin and mounted in neutral balsam medium (Sinopharm Chemical).

Immunohistochemistry analysis for RIPK3 or p-S164/T165-RIPK3 was performed using an antibody against RIPK3 and p-S164/T165-RIPK3. Primary antibody against Cleaved-Caspase3 or p-S164/T165-RIPK3 was incubated overnight at 4°C in PBS. After 3 washes with PBS, slides were incubated with DyLight-555/488 conjugated donkey anti-rabbit/mouse secondary antibodies (Thermo Fisher) in PBS for 8 h at 4°C. After a further 3 washes, slides were incubated with RIPK3 or p-S164/T165-RIPK3 antibody

overnight at 4°C in PBS. After a further 3 washes, slides were incubated with DyLight-488/555 conjugated donkey anti-mouse/rabbit secondary antibodies (Thermo Fisher) for 2 hours at room temperature in PBS. After a further 3 washes in PBS, the cell nuclei were then counterstained with DAPI (Thermo Fisher) in PBS. Fluorescence microscopy was performed using a Nikon A1-R confocal microscope.

Isolation of mice granulosal lutein cells from ovaries (Newton et al., 1999; Tian et al., 2015)

Ovaries from 3-month old wild-type mice were collected and placed in Enriched DMEM:F12 (Hyclone) media and placed on ice. Ovaries were ground on the strainer (40 μm) with forceps. Centrifuge the cell suspension at 900 × g for 5 min at 4°C, wash 3 times with PBS. The mix cells pellet were incubated with trypsin for 15-20 min at 37°C in a shaking water bath at 80 oscillations (osc)/min and were then layered over 40 mL 5% Percoll/95% 1× Hank's balanced salt solution in a 50 mL conical tube and allowed to settle for 20 min. After incubation, 3 mL charcoal-stripped FBS was immediately added to halt the digestion. All fractions were mixed and immediately centrifuged at 900 × g for 10 min at 4°C. Pellets were re-suspended in PBS and washed 3 times, then cultured in DMEM:F12 (10%FBS) medium at 37°C with 5% CO_2. After 24 h, the suspended granulosal lutein cells were collected and cultured in a new cell dish, and the cells were treated with the indicated stimuli. The adherent follicular granulosa cells were collected and were treated with the indicated stimuli. Cell lysates were analyzed by western blotting.

***In vivo* studies of luteal regression** (Carambula et al., 2002; Carambula et al., 2003)

Wild-type, *Ripk3*$^{-/-}$, *Fadd*$^{-/-}$*Mlkl*$^{-/-}$, *Ripk3*$^{S165A\text{-}T166A/\ S165A\text{-}T166A}$ and *Ptgfr*$^{-/-}$ female mice (each group, n=16) at day 25-26 postpartum were intraperitoneally injected with 7.5 IU (100 μl/mouse) pregnant mare serum gonadotropin (PMSG) followed by intraperitoneal injection with 7.5 IU (100 μl/mouse) serum gonadotropin and chorionic gonadotropin (SCG) 46 h later to induce superovulation. Those mice were injected with Dinoprost Tromethamine (DT) (10 micrograms, i.p.) or saline at 24 h after post-ovulation. Ovaries were then collected at 12 or 24 h post-injection. In some experiments, ovaries were ground and re-suspended in lysis buffer, homogenized for 30 seconds with a Paddle Blender (Prima, PB100), incubated on ice for 30 min, and centrifuged at 20,000 × g for 30 min. The supernatants were analyzed by western blotting. In other experiments, ovaries were fixed with 4% paraformaldehyde, paraffin-embedded, serially sectioned (5 μm), and mounted in order on glass microscope slides. Ovarian mid-sagittal sections were used for immunohistochemical analysis with RIPK3 or cleaved-caspase3 antibody.

Mass spectrometry and data analysis

HeLa/TO-RIPK3 and MCF7/TO-RIPK3 cells were treated with Dox plus z-VAD for 24 hours. Then the cell extracts were prepared and used for immunoprecipitation with an anti-Flag antibody. The immunoprecipitates were washed three times with lysis buffer. The beads were then eluted with 0.5 mg/mL of the corresponding antigenic peptide for 6 hours or directly boiled in 1× SDS loading buffer and subjected to SDS-PAGE. RIPK3 bands were excised from SDS-PAGE gel and then dissolved in 2M urea, 50 mM ammonium bicarbonate, pH 8.0, and reduced in 2 mM DTT at 56 ℃ for 30 min followed by alkylation in 10 mM iodoacetamide at dark for 1 hr. Then the protein was digested with sequencing grade modified trypsin (Promega) (1: 40 enzyme to total protein) at 37 ℃ overnight. The tryptic peptides were separated by an analytical

capillary column (50 μm × 15 cm) packed with 5 μm spherical C18 reversed phase material (YMC, Kyoyo, Japan). A Waters nanoAcquity UPLC system (Waters, Milford, USA) was used to generate the following HPLC gradient: 0-30% B in 40 min, 30-70% B in 15 min (A = 0.1% formic acid in water, B = 0.1% formic acid in acetonitrile). The eluted peptides were sprayed into a LTQ Orbitrap Velos mass spectrometer (ThermoFisher Scientific, San Jose, CA, USA) equipped with a nano-ESI ion source. The mass spectrometer was operated in data-dependent mode with one MS scan followed by four CID (Collision Induced Dissociation) and four HCD (High-energy Collisional Dissociation) MS/MS scans for each cycle. Database searches were performed on an in-house Mascot server (Matrix Science Ltd, London, UK) against Human RIPK3 protein sequence. The search parameters are: 7 ppm mass tolerance for precursor ions; 0.5 Da mass tolerance for product ions; three missed cleavage sites were allowed for trypsin digestion and the following variable modifications were included: oxidation on methionine, cysteine carbamidomethylation, and serine, threonine, and tyrosine phosphorylation.

Statistical analysis

All experiments were repeated at least twice, with similar results. Data represent biological replicates. Statistical tests were used for every type of analysis. The data meet the assumptions of the statistical tests described for each figure. Results are expressed as the mean ±s.e.m or S.D. Differences between experimental groups were assessed for significance using a two-tailed unpaired Student's t-test using GraphPad prism5 and Excel software. The $*P<0.05$, $**P<0.01$, and $***P<0.001$ levels were considered significant. NS, not significant.

Acknowledgements

We thank Dr. Alex Wang for critically reading and editing the manuscript. This work was supported by institutional grants from the Chinese Ministry of Science and Technology and Beijing Municipal Commission of Science and Technology. The funders had no role in study design, data collection and interpretation, or the decision to submit the work for publication.

Author contributions

D.L. and X.W. designed the research and analyzed the data. D.L. conducted majority of the experiments. J.C., and J.G. conducted cell death and IHC experiments. L.L., G.C., Y.C. carried out mass spectrometry analysis. Y.Z. and F.W. generated PTGFR knockout mice and helped with in vivo studies of luteal regression experiments. D.L. and X.W. wrote the manuscript.

Figure 1

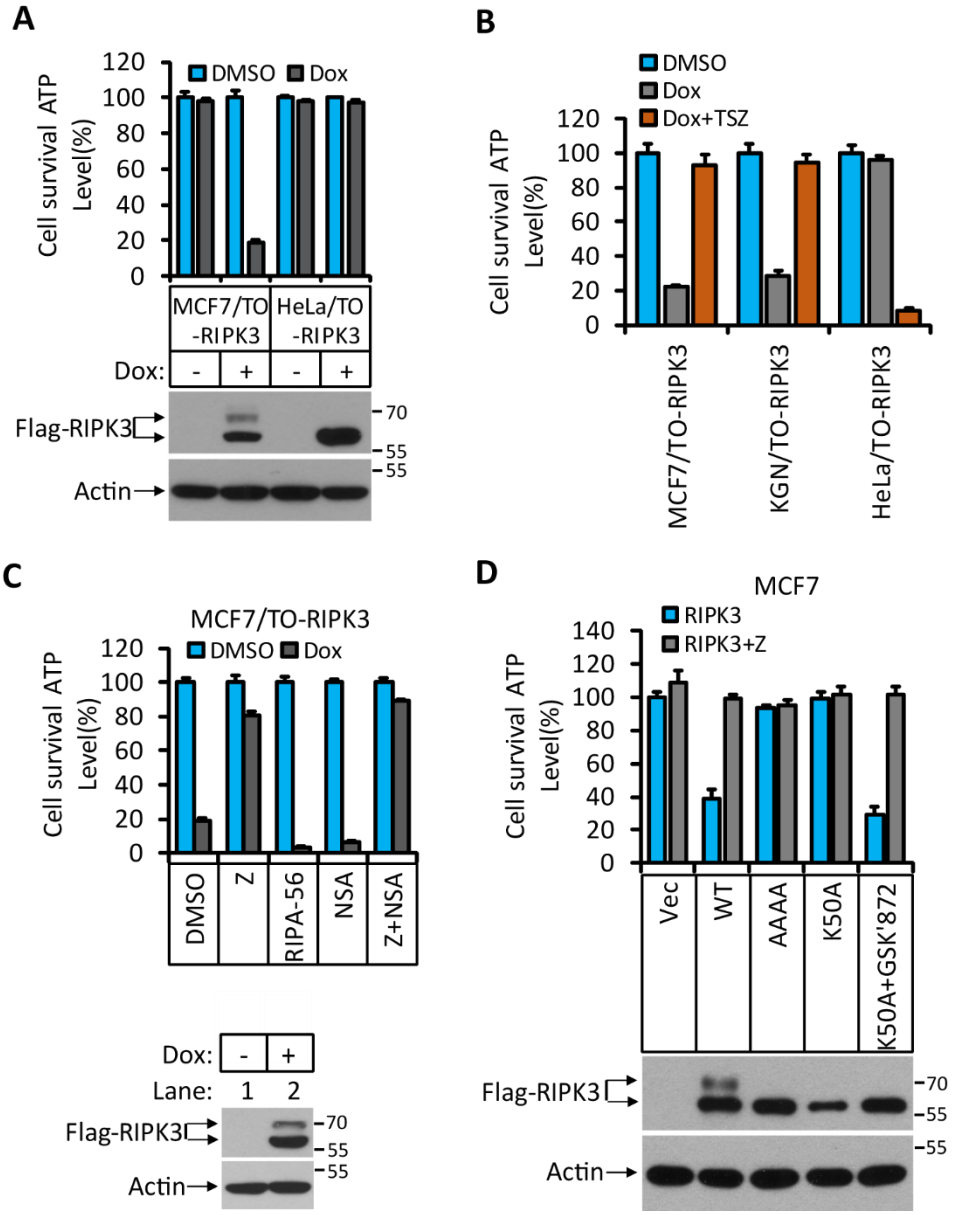

Figure 2

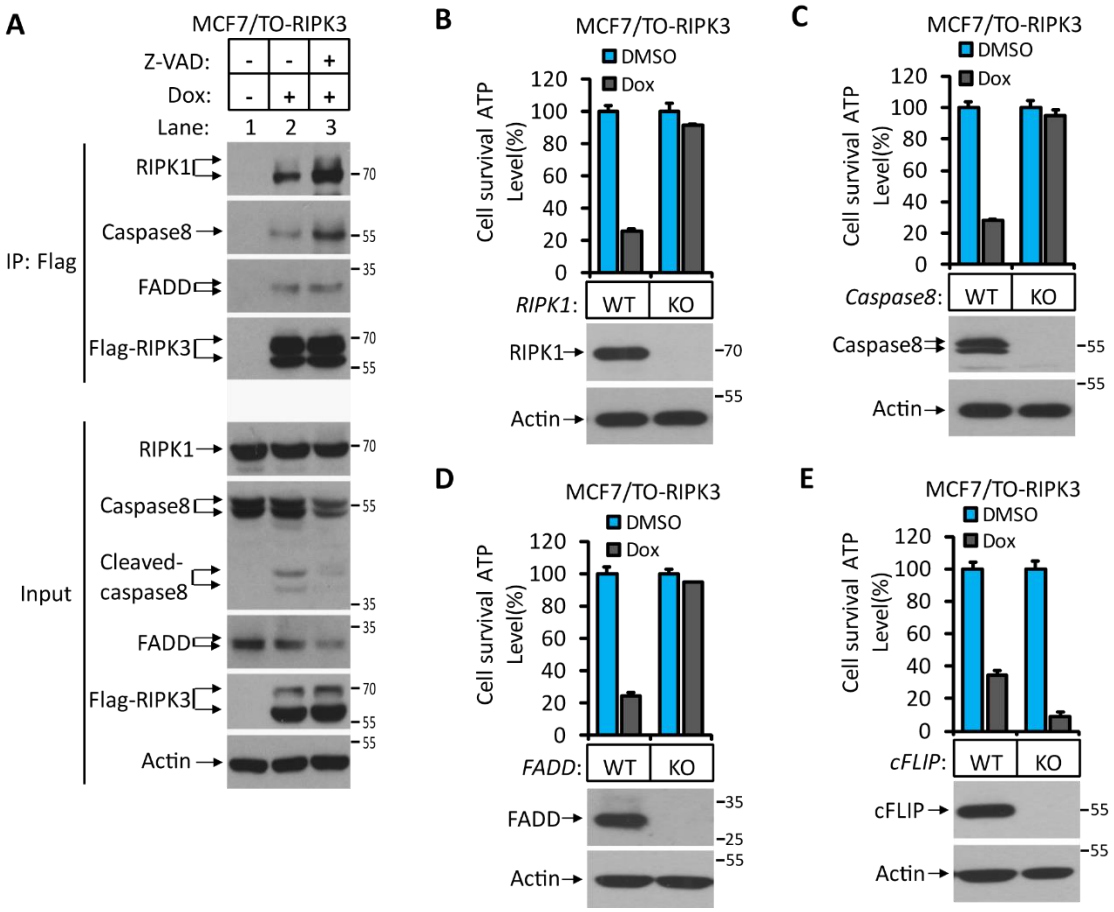

Figure 3

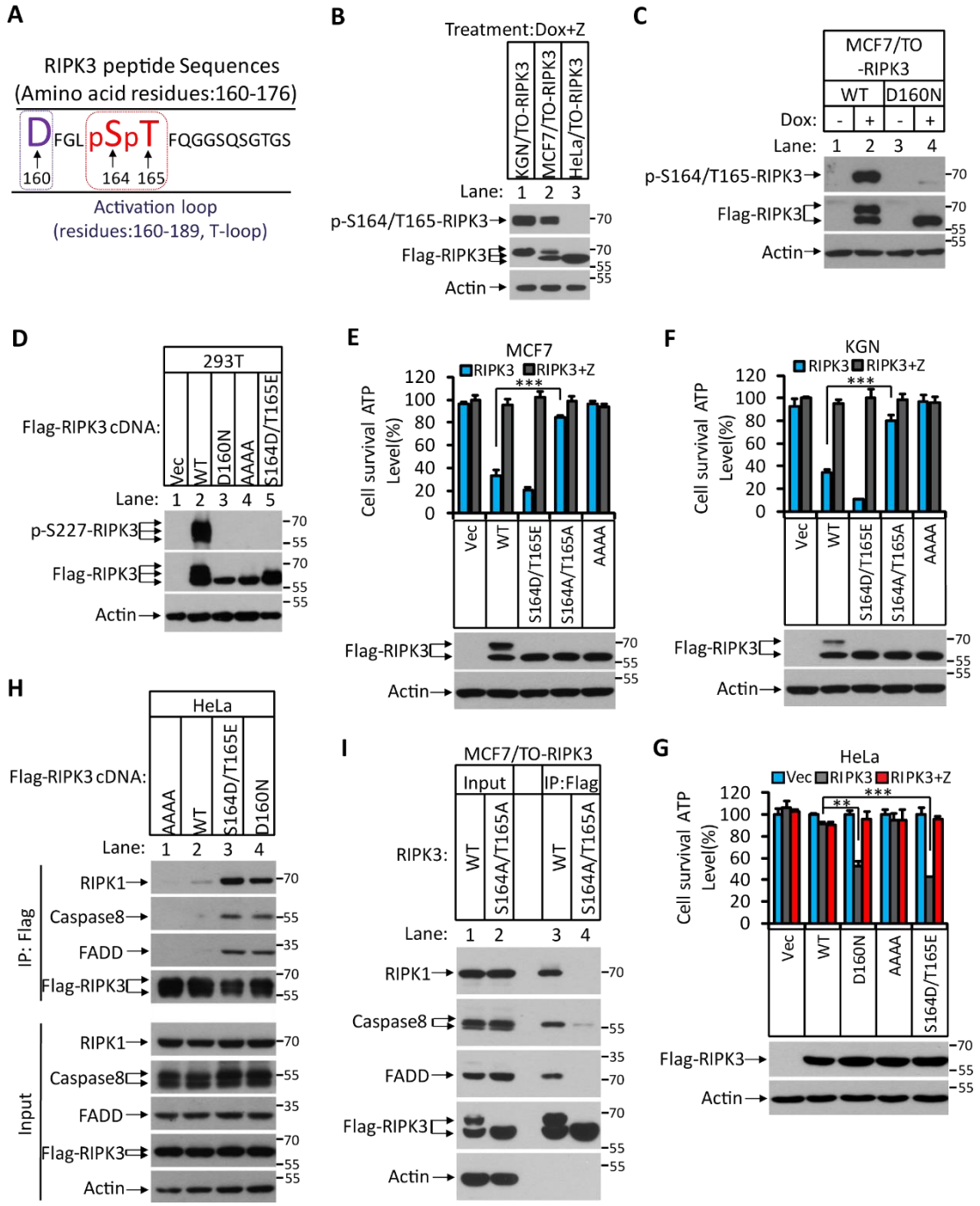

Figure 4

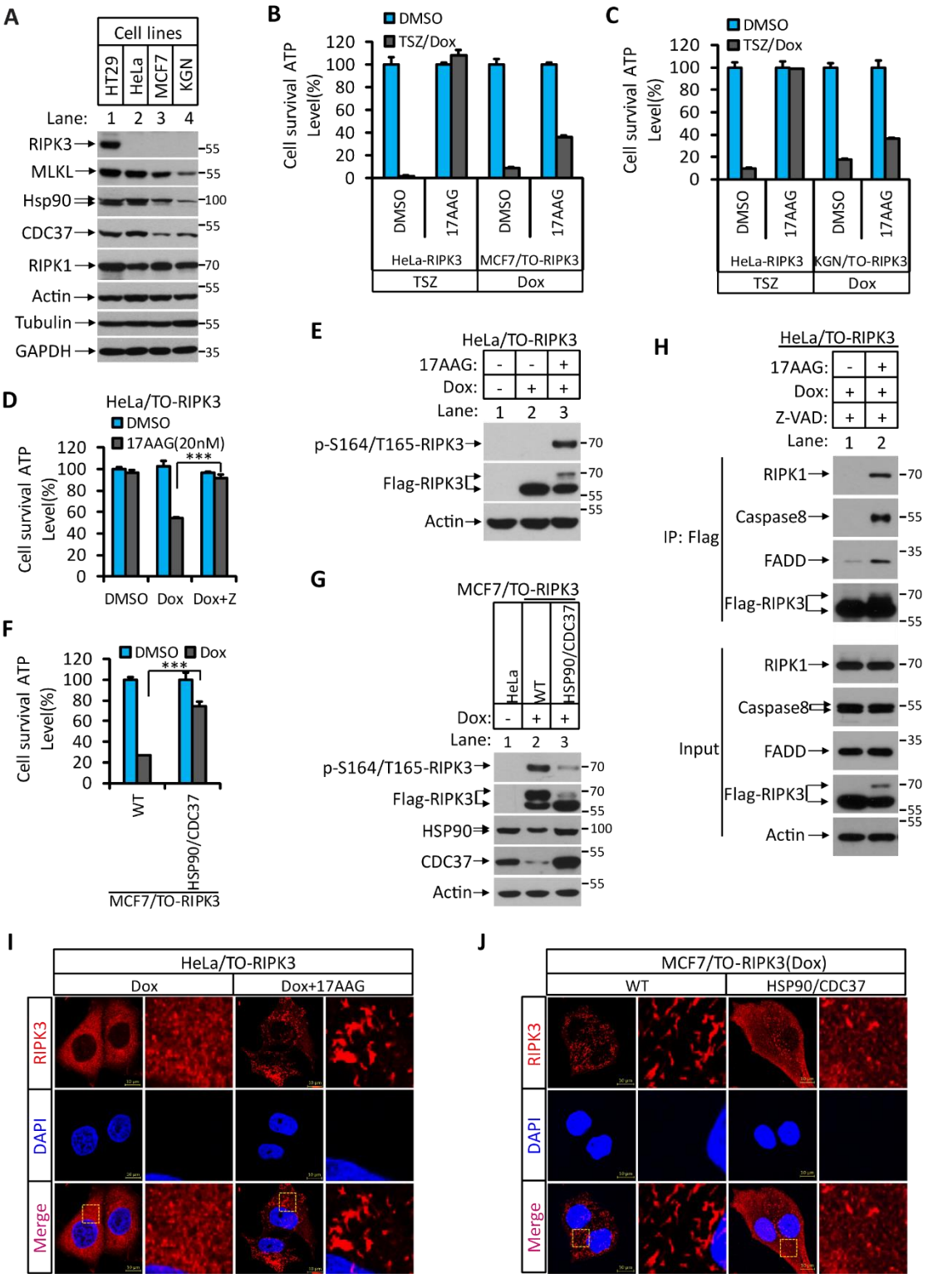

Figure 5

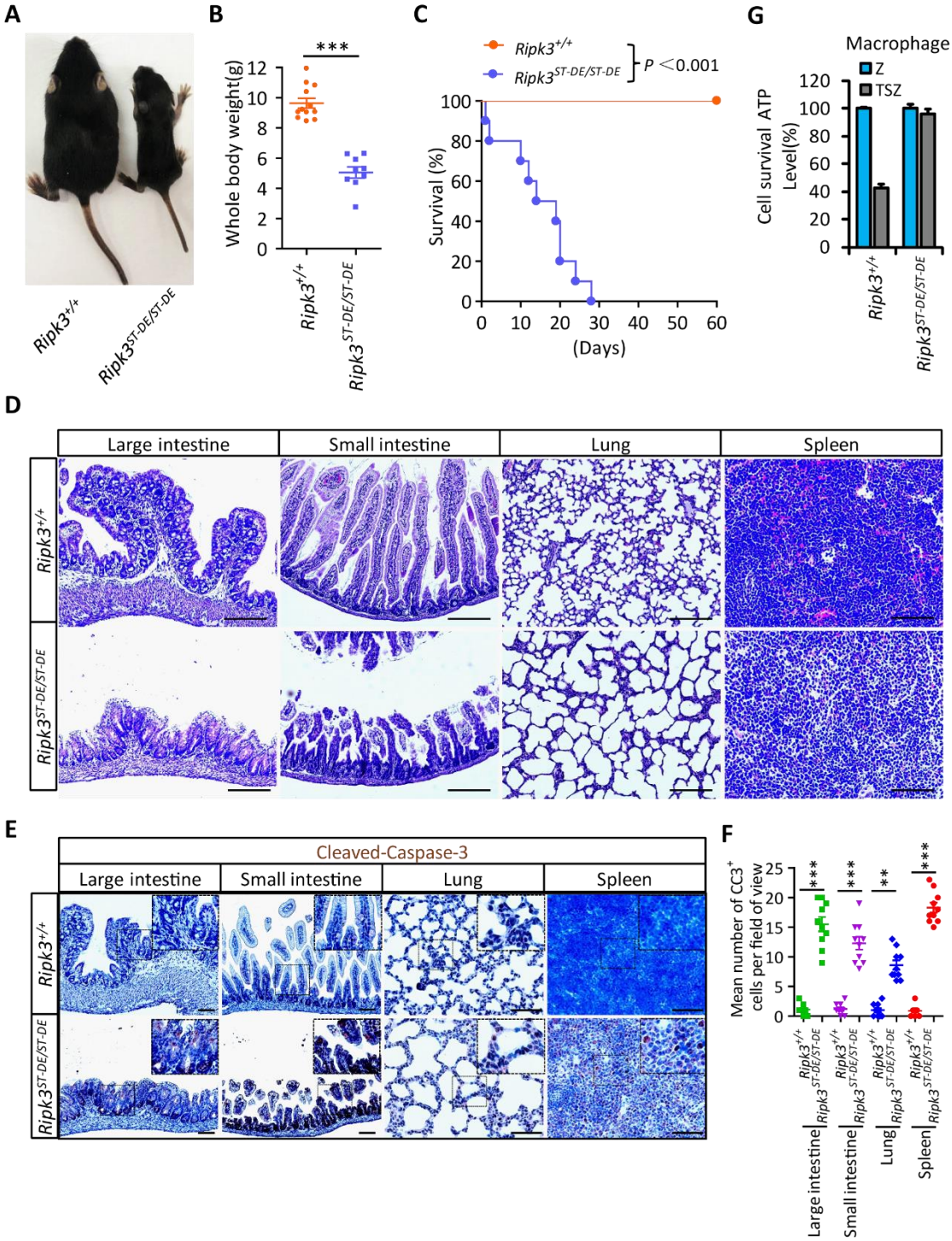

Figure 6

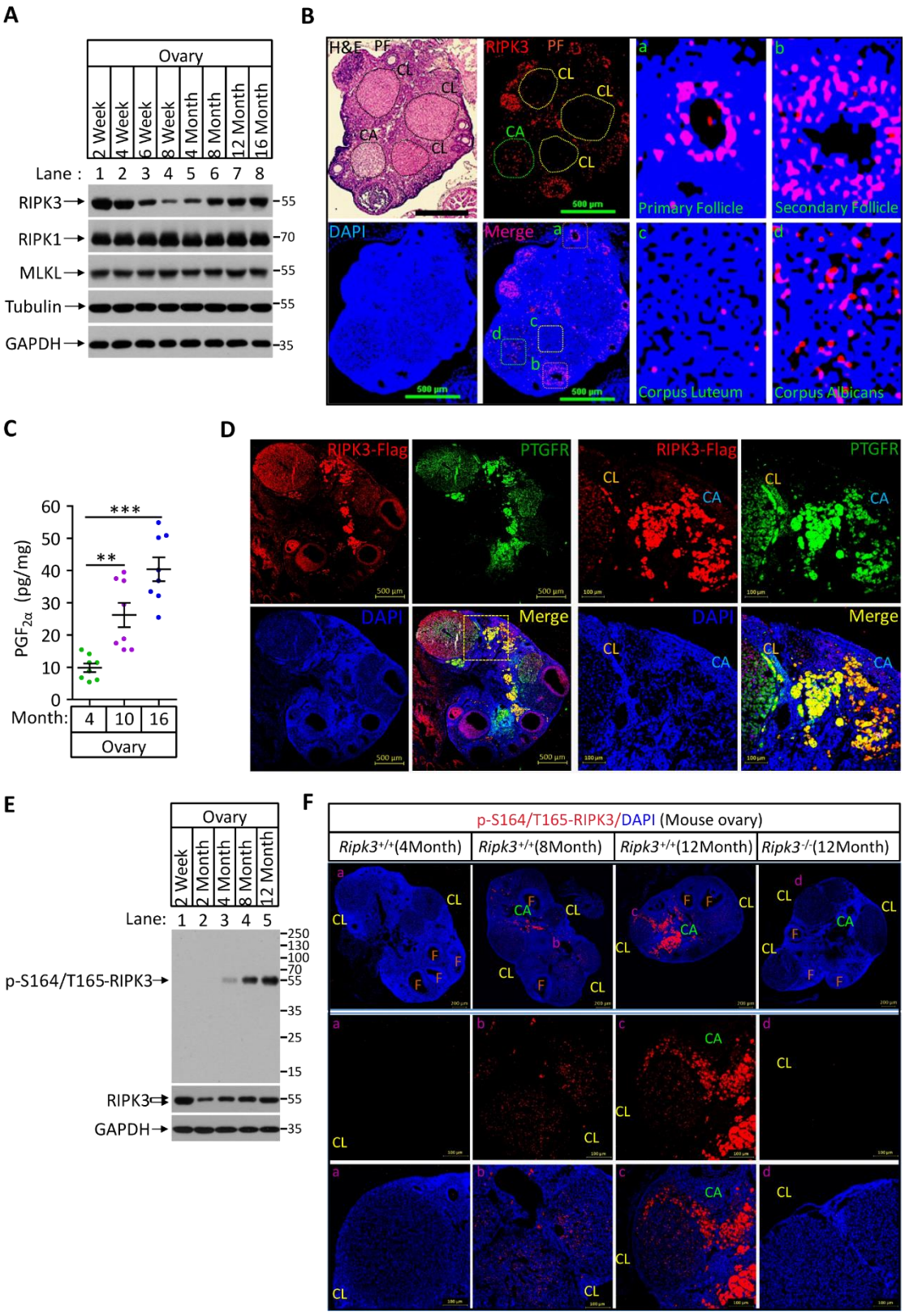

Figure 7

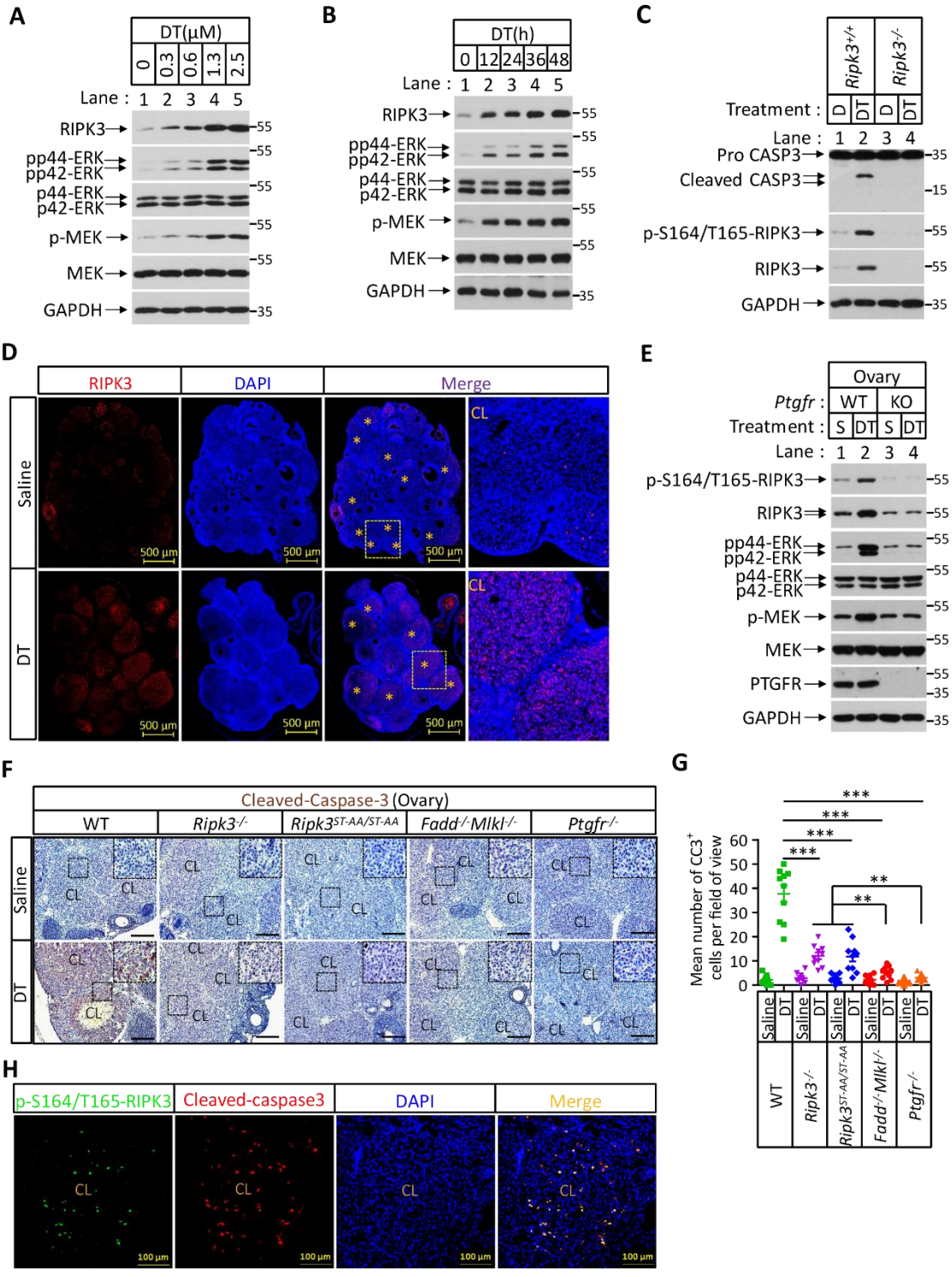

Figure 1-figure supplement 1

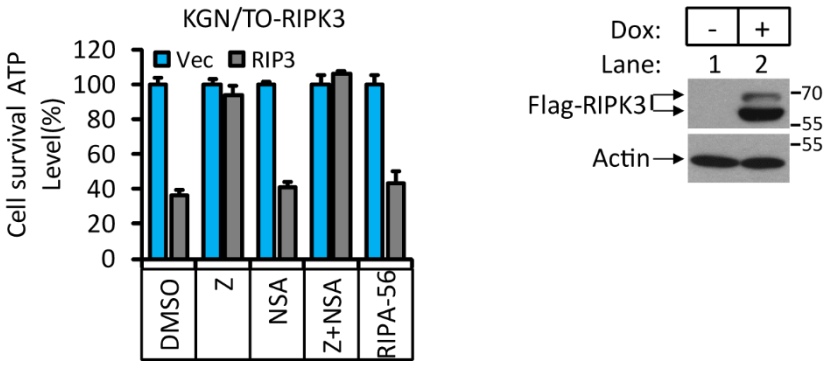

Figure 3-figure supplement 1

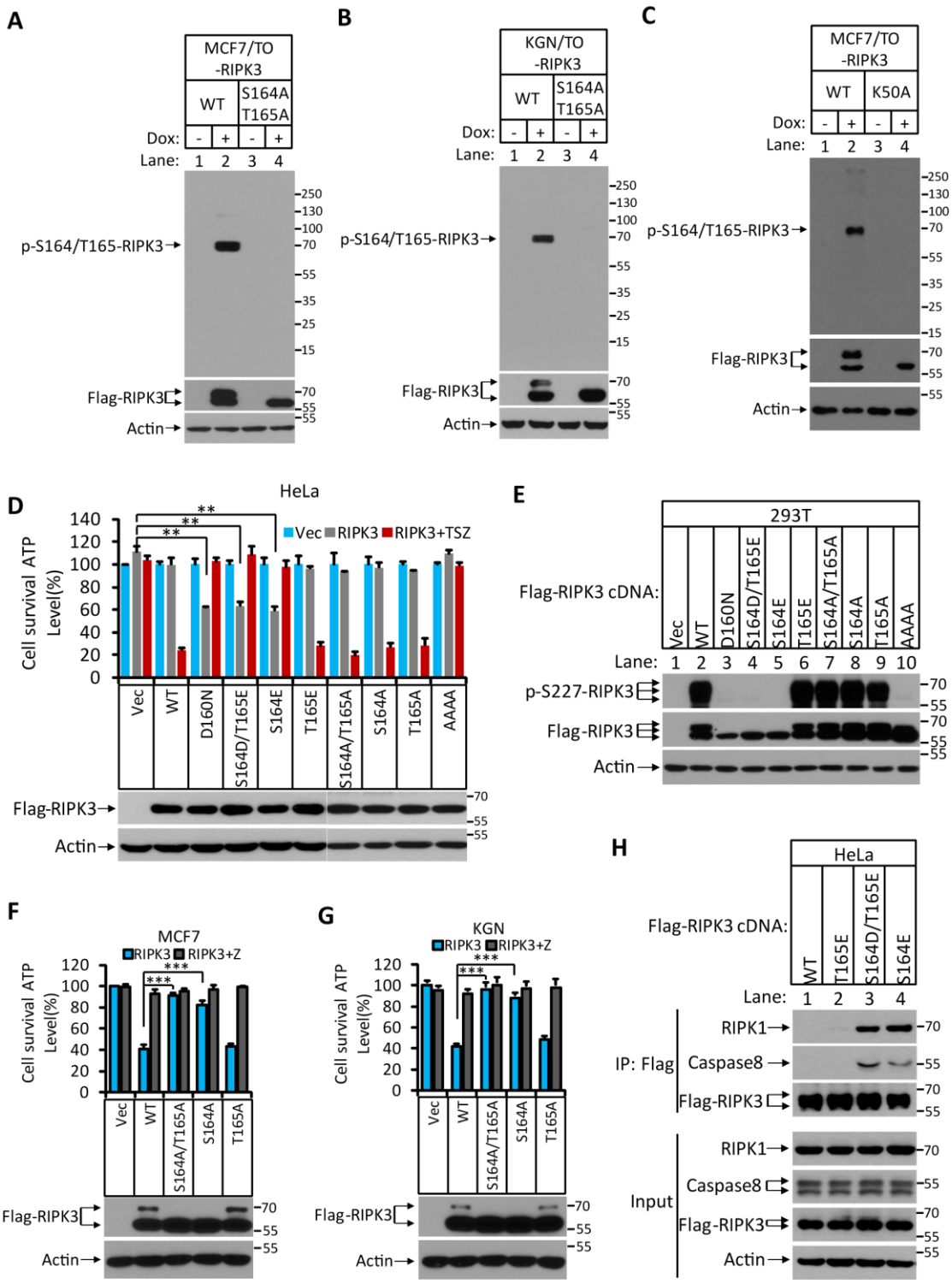

Figure 3-figure supplement 2

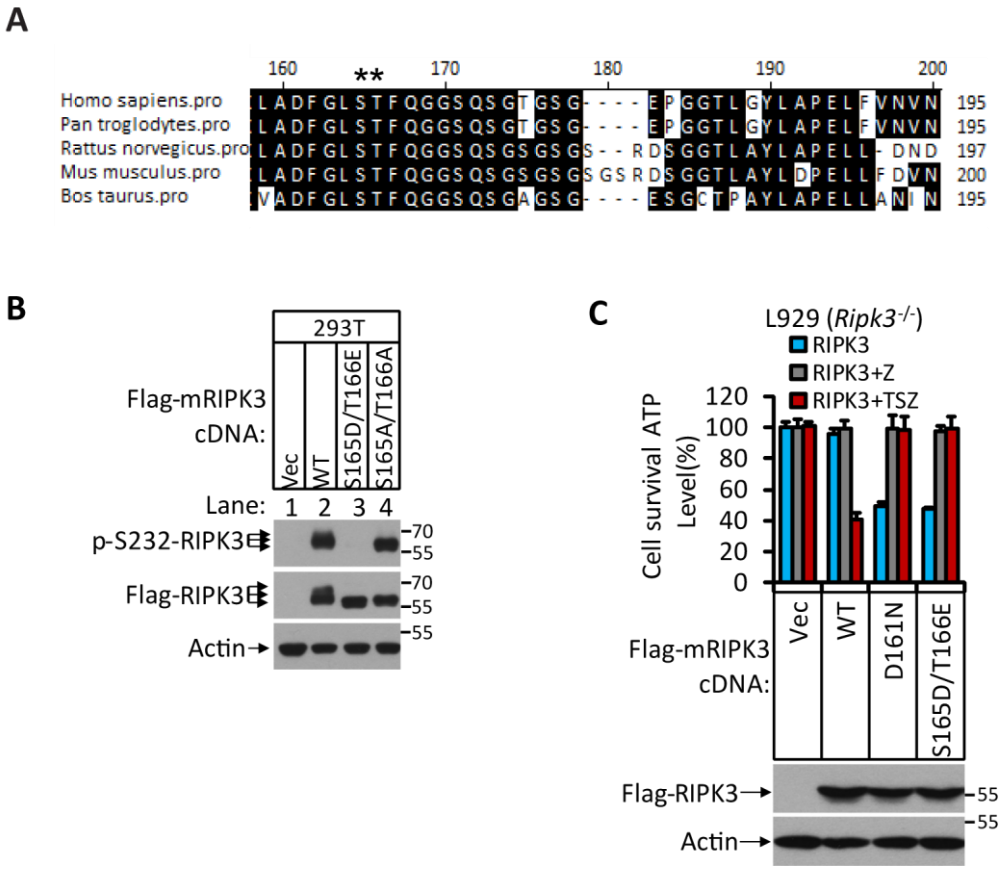

Figure 4-figure supplement 1

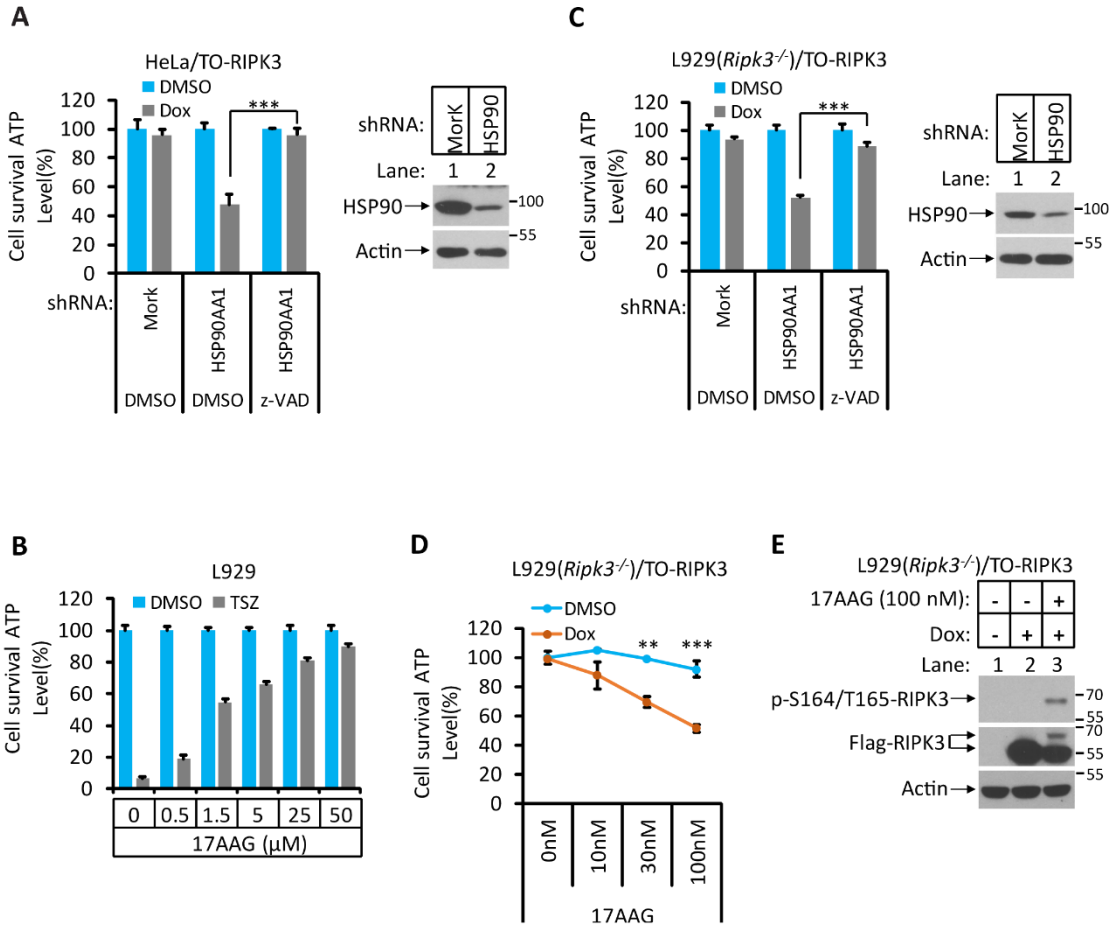

Figure 4-figure supplement 2

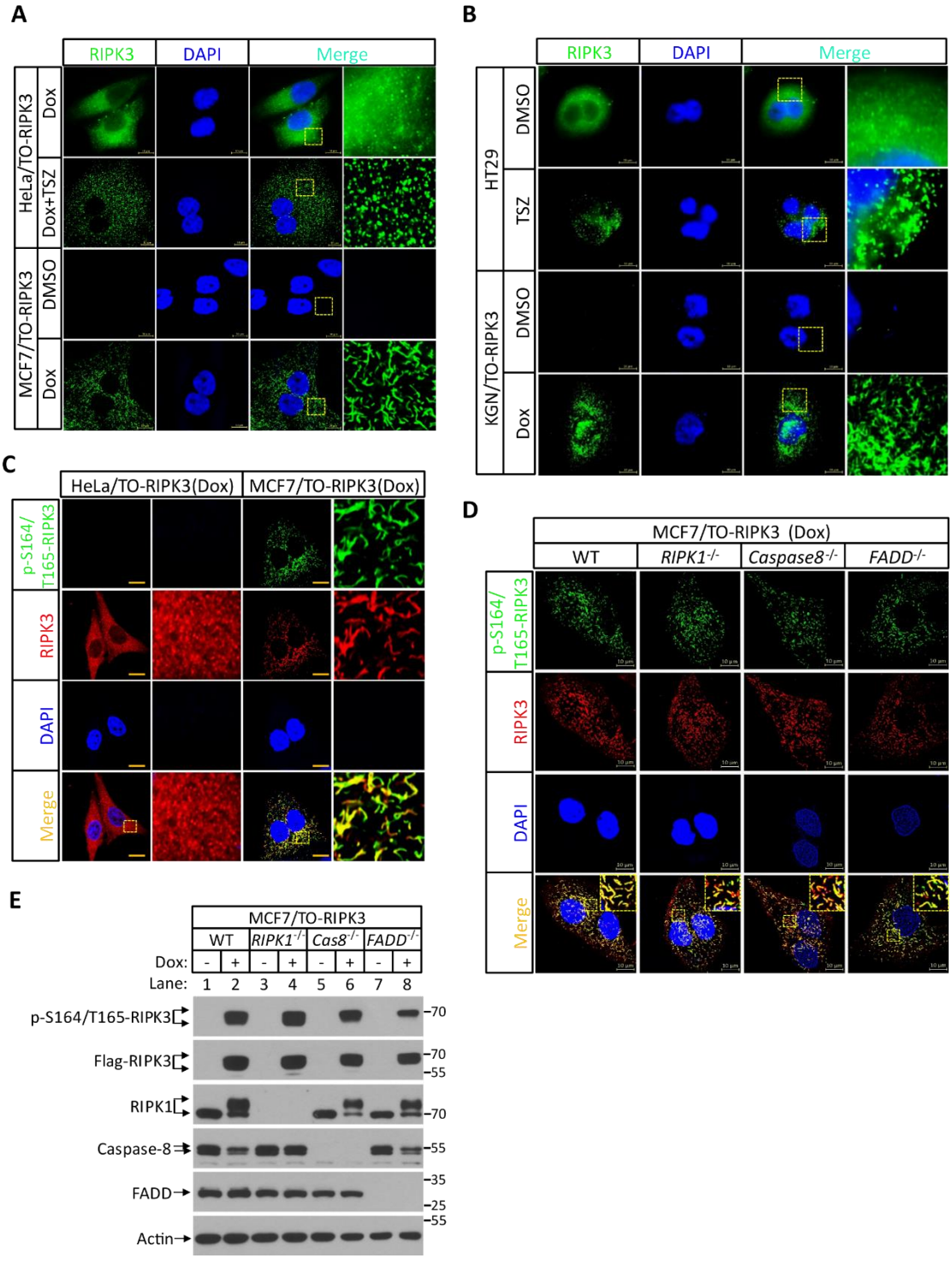

Figure 4-figure supplement 3

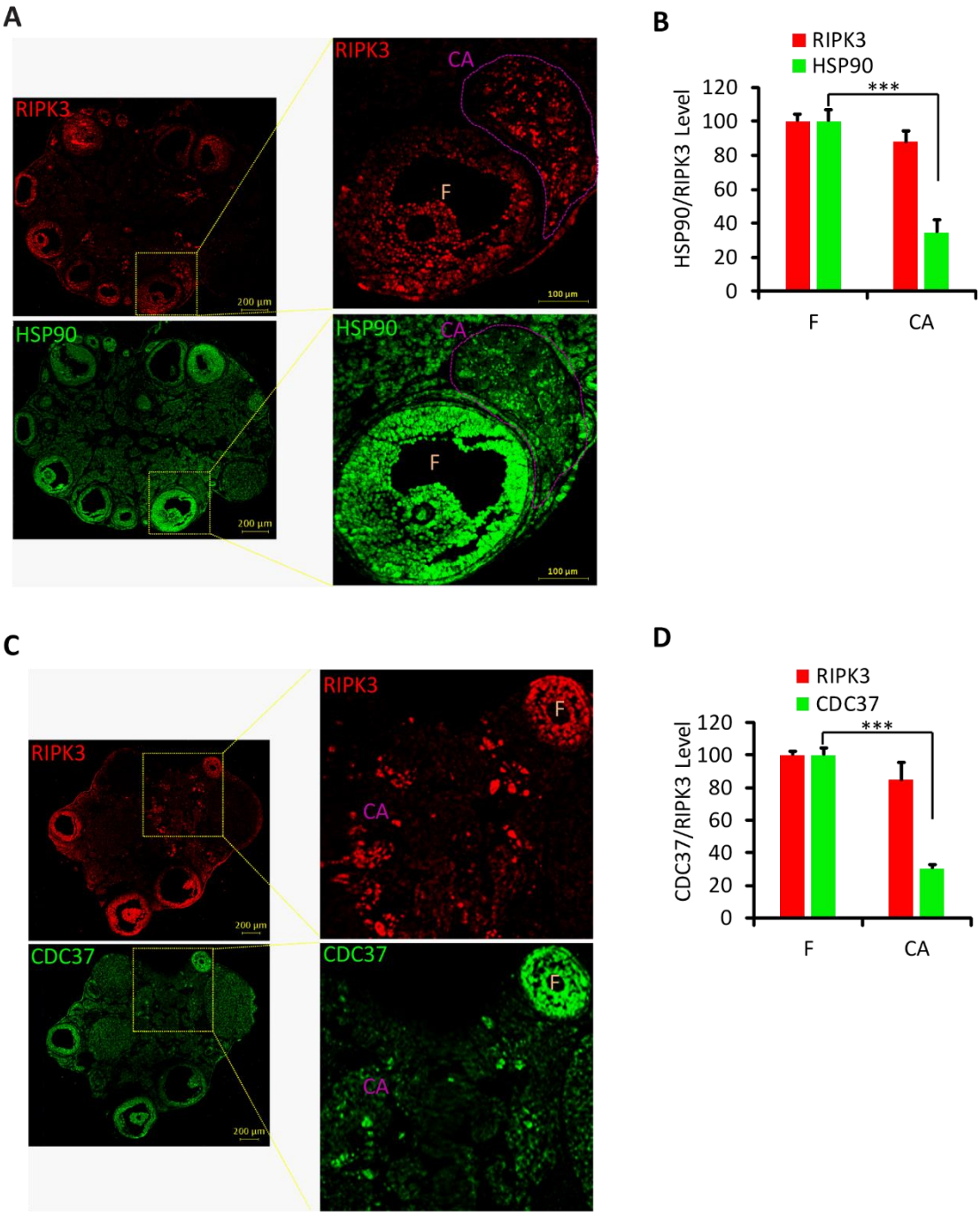

Figure 5-figure supplement 1

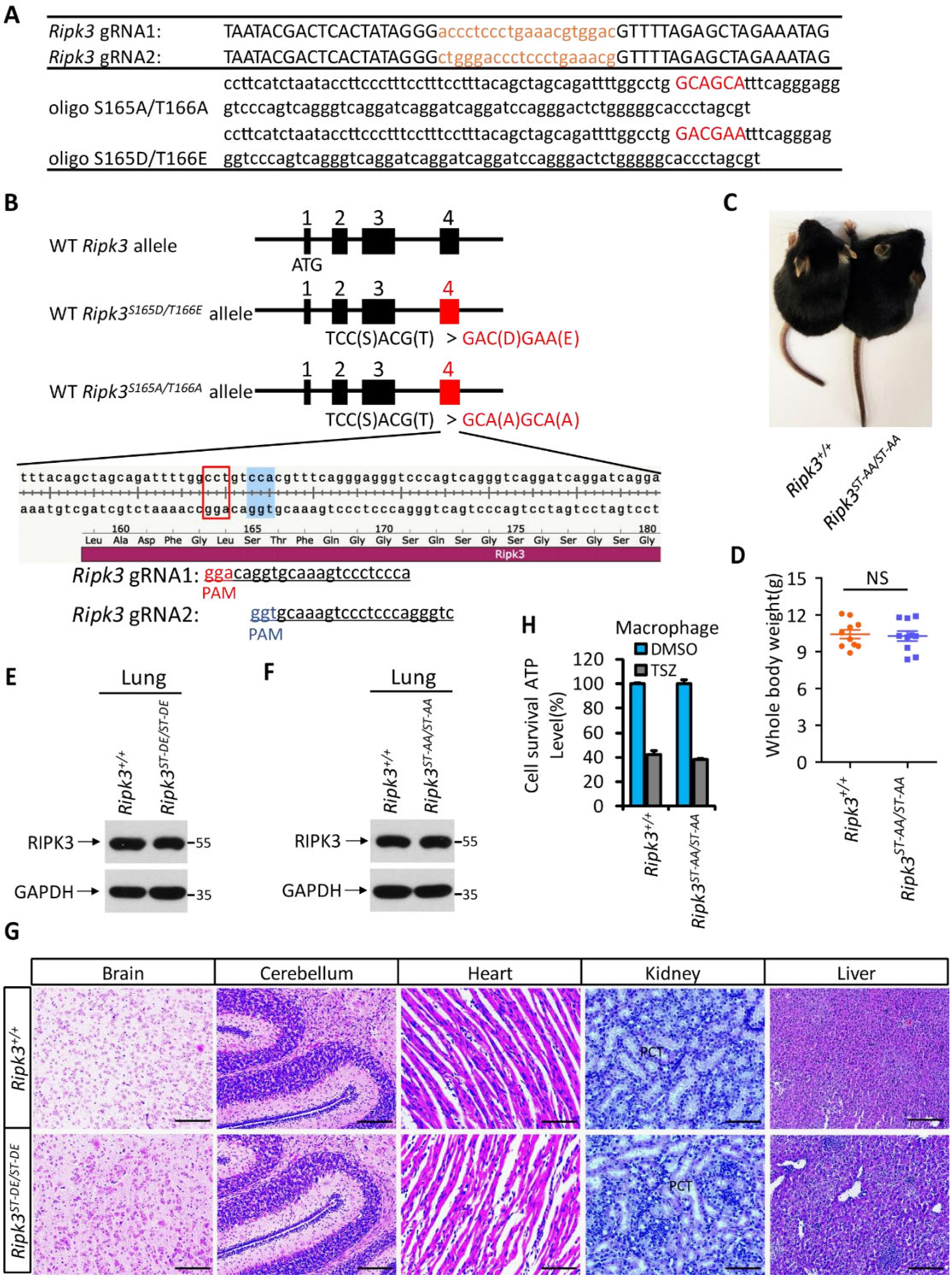

Figure 6-figure supplement 1

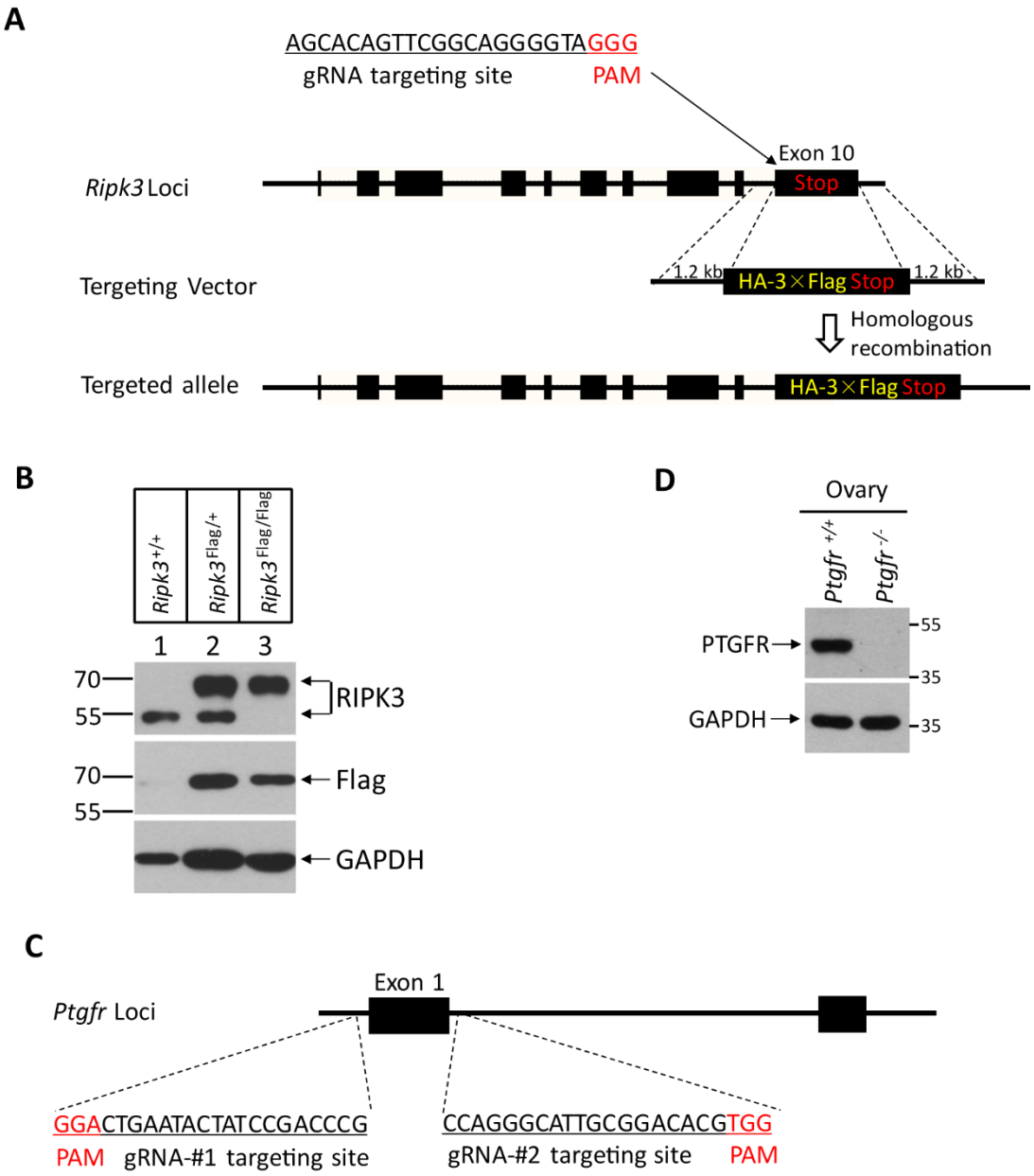

Figure 7-figure supplement 1